Tampere University

Saana Seppälä

DEVELOPING GLUTAMATE UPTAKE MODEL FOR NEURON-ASTROCYTE SYNAPSE

Master of Science (Tech.) Thesis
Faculty of Medicine and Health Technology
Examiners: Dos. Jussi Koivumäki
Dos. Marja-Leena Linne
November 2022

ABSTRACT

Saana Seppälä: Developing Glutamate Uptake Model for Neuron-Astrocyte Synapse
Master of Science (Tech.) Thesis
Tampere University
Master's Programme in Biotechnology and Biomedical Engineering
November 2022

The two most abundant cell types in the brain are neuronal cells and non-neuronal glial cells. Both cell types can form extensive networks of their own, but they also interact with each other. Recently in the field of neuroscience, glial cells have been recognized to have significantly larger roles in the central nervous system, compared to the previously thought roles in homeostasis and as supporting cells. As an example, glial cells have been shown to participate in sensory information processing and higher brain functions. One specialized subtype of glial cells is astrocytes. Astrocytes have been shown to be closely associated with neuronal synapses and to participate in the regulation of synaptic functions and plasticity. The interactions between neurons and astrocytes in the brain are driven by many complex cellular mechanisms. Such mechanisms include, for example, exocytosis and uptake of transmitters and other molecules.

One important form of interaction between neurons and astrocytes at the synaptic level is glutamate uptake. Glutamate is an excitatory neurotransmitter, released into the synaptic cleft by neurons. Excess glutamate in the synaptic cleft can lead to neurotoxic reaction, such as epileptic seizures, so the glutamate concentration must be carefully modulated. It has been shown that most of the glutamate uptake is carried out by astrocytes. Astrocytes actively control the glutamate dynamics in the synaptic cleft by taking up glutamate through specific glutamate transporters, and releasing it to the extrasynaptic space.

In this thesis work, a previously published and validated synapse model was further developed to incorporate a direct pathway for astrocytic glutamate uptake from the synaptic cleft. The previous model described dynamics in a specific synapse in somatosensory cortex, where evidence of astrocytes modulating synaptic plasticity has previously been found. The new model component for astrocytic glutamate uptake dynamics was developed based on a comprehensive survey and literature search of astrocytic glutamate transporter models. Due to the level of complexity and the biophysical nature of the original synapse model, it was of interest to reconcile whether it is even possible to integrate this mechanism.

The simulation results obtained with the new implementation of the model were promising, since the new model was reasonably fitted to produce results close to those of the original model. The successful integration of the glutamate uptake component made it possible to perform further simulations to study the behavior of the new model. The dynamics and results of the new model are related to the ability of the synapse to learn and modulate sensory information, making the model a viable tool for further research on the role of astrocytic glutamate uptake. It was of importance to introduce a fully replicable model code, thus all new and modified mathematical expressions and implementation details are presented.

Keywords: astrocyte, glutamate transporter, modeling, neuron, synapse

TIIVISTELMÄ

Saana Seppälä: Glutamaatin sisäänottomallin kehittäminen hermosolu-astrosyyttisynapsille
Diplomityö
Tampereen yliopisto
Bioteknologian ja biolääketieteen tekniikan maisteriohjelma
Marraskuu 2022

Aivojen kaksi ensisijaista solutyyppiä ovat hermosolut ja gliasolut. Molemmat solutyypit voivat muodostaa laajoja solutyypin sisäisiä verkostoja, mutta ne vaikuttavat myös keskenään yli solutyyppirajojen. Viime aikoina neurotieteen alalla gliasoluilla on tunnistettu olevan huomattavasti suurempi rooli keskushermostossa, aiemmin tunnistettuihin homeostaattisiin ja tukirooleihin verrattuna. Nykytiedon mukaan gliasolut osallistuvat sensorisen informaation käsittelyyn sekä korkeampiin aivotoimintoihin. Yksi erikoistunut gliasolujen alatyyppi ovat astrosyytit. Astrosyyttien on osoitettu sijaitsevan lähellä hermosolujen synapseja, ja osallistuvan synapsin toiminnan säätelyyn sekä synaptiseen muovautuvuuteen. Hermosolujen ja astrosyyttien tiedetään vuorovaikuttavan keskenään monella eri kompleksisella tavalla, hyödyntäen muun muassa välittäjäaineiden sekä muiden molekyylien eksosytoosia sekä sisäänottoa.

Glutamaatin sisäänotto on yksi tärkeä hermosolujen ja astrosyyttien välisen vuorovaikutuksen muoto synapsitasolla. Glutamaatti on eksitatorinen hermovälittäjäaine, jota neuronit vapauttavat synapsirakoon. Ylimääräinen glutamaatti synapsiraossa voi johtaa neurotoksiseen tilaan, joten sopivaa glutamaattipitoisuutta tulee ylläpitää tarkasti. Astrosyyttien on osoitettu huolehtivan suurimmasta osasta glutamaatin sisäänotosta synapsiraossa. Astrosyytit kontrolloivat aktiivisesti synapsin glutamaattidynamiikkaa ottamalla glutamaattia sisään erikoistuneiden glutamaattitransporttereiden avulla ja vapauttamalla sitä solunulkoiseen tilaan.

Tässä opinnäytetyössä jatkokehitettiin aiemmin julkaistua ja validoitua synapsimallia, tarkoituksena luoda malliin uusi komponentti kuvaamaan glutamaatin sisäänottoa astrosyyttiin. Kyseinen, aiemmin julkaistu malli kuvaa spesifistä synapsia somatosensorisella korteksilla, jossa on aiemmin havaittu todisteita astrosyyttien roolista synaptisessa muovautuvuudessa. Kyseinen komponentti astrosyytin glutamaatin sisäänotolle luotiin kattavan tutkimuksen perusteella, jossa analysoitiin julkaistuja, astrosyyttien glutamaattitransporttereita hyödyntäviä malleja. Alkuperäisen synapsimallin monimuotoisen biofysikaalisen ja -kemiallisen luonteen johdosta työn ensisijainen tavoite oli selvittää, mikäli kyseinen mekanismi on edes mahdollista implementoida alkuperäiseen malliin.

Uutta, jatkokehitettyä mallia simuloimalla saatiin lupaavia tuloksia, sillä uuden mallin toiminta voitiin realistisesti sovittaa tuottamaan alkuperäistä mallia vastaavia tuloksia. Glutamaatin sisäänottokomponentin onnistunut integroiminen mahdollisti myös sen, että kehitetyn mallin toiminnan tutkimiseen voitiin syventyä hieman lisää. Kehitetyllä mallilla saadut tulokset kuvaavat synapsin kykyä oppia sekä muokata sensorista informaatiota. Näiden tulosten perusteella mallia voidaan hyödyntää työkaluna myös myöhemmissä astrosyytin glutamaatin sisäänottoa koskevissa tutkimuksissa.

Avainsanat: astrosyytti, glutamaattitransportteri, hermosolu, mallintaminen, synapsi

PREFACE

This Master's Thesis in the Biotechnology and Biomedical Engineering programme was done in the Computational Neuroscience Research Group at Tampere University. I would especially want to thank my supervisors, Dos. Marja-Leena Linne and D.Sc. Tiina Manninen, for providing me great guidance for the practical and written part of the work, throughout the process. I want to thank my supervisors also for giving me the possibility to challenge myself with an interesting topic.

Finally, I would like to thank all the members of the Computational Neuroscience group for helping with the finishing touches of the work, and especially Sofia Ylihärsilä for contributing to the discussion and evaluation of the biological details of the published glutamate transporter models.

Tampere, 11th November 2022

Saana Seppälä

CONTENTS

LIST OF ABBREVIATIONS

2-AG	2-arachadonylglycerol
AMPAR	α-amino-3-hydroxy-5-methyl-4-isoxazole propionic acid receptor
ATP	Adenosine triphosphate
CaN	Calcineurin
CNS	Central nervous system
EAAT	Excitatory Amino Acid Transporter
ER	Endoplasmic reticulum
GABA	Gamma-aminobutyric acid
GluT	Glutamate transporter
HH-model	Hogdkin-Huxley model
IP_3	Inositol trisphosphate
LTD	Long-term depression
LTP	Long-term potentiation
mGluR	Metabotropic glutamate receptor
NKA	Na^+/K^+-ATPase
NMDAR	N-methyl-D-aspartate receptor
ODE	Ordinary differential equation
PDS	Paroxysmal depolarization shifts
RSD	Recurrent spreading depolarization
SDE	Stochastic differential equation
SERCA	Sarco/ER Ca^{2+}-ATPase pump
STDP	Spike-timing-dependent plasticity
t-LTD	Spike-timing-dependent long-term depression
t-LTP	Spike-timing-dependent long-term potentiation

1. INTRODUCTION

The two primary cell types in the central nervous system (CNS) are considered to be neurons and glia [1], although it is still a debate which cell type is more abundant. Currently, the glia/neuron ratio is known to vary between different brain regions, developmental stages and animals. Generally, the bigger the brain, the bigger the neurons, resulting in smaller density of neuronal cells and thus higher glia/neuron ratio [2]. Some experimental studies have presented ratios varying from 0.3 in rodents to 1.5 in humans [3, 4]. However, these are still estimates, and we are yet to be able to make any definite conclusions about the ratio [5].

For many years glial cells were thought to be merely supporting cells for neurons, like "brain glue" [6]. The wide range of glial functions have since been recognized, and glial research has drawn more interest in recent years. One subtype of glial cells, the astrocytes, has attracted particular attention. Several important functions for astrocytes have been found outside previously noted homeostatic and supporting roles. Also, more controversial roles of astrocytes have been suggested, particularly related to synaptic transmission and plasticity as well as memory and learning [7, 8]. To study the diverse functions of astrocytes in the brain, it is of interest to study their interaction with neurons. One way to study these interactions is to develop mathematical models and tools for computational neuroscience.

Computational neuroscience is a field under neuroscience, which uses mathematical tools and expressions to study and understand the nervous system in health and disease [1, 9]. Computational neuroscience is closely considering experimental neuroscientific data, which is of great importance for constructing and validating the dynamical behavior of mathematical models. Computational modeling of astrocytes has not yet reached the level of modeling neurons. Astrocytes do not fire action potentials, so gathering experimental data for astrocytes, for example for validating the models, is more challenging compared to neuronal data. Despite the challenges, it is of interest to create more precise and efficient models incorporating also astrocytic components, following the increased knowledge on the importance of astrocytes in normal brain functions. By mathematically describing the experimental findings, computational modeling could help to tackle the challenges in the astrocyte research.

One important function of astrocytes to incorporate into the models is the uptake of the most abundant excitatory neurotransmitter in the central nervous system, the glutamate. Glutamate uptake is a cellular process which controls regional concentrations of glutamate. Astrocytic glutamate uptake is known to have a crucial role in maintaining the normal brain functions. Excessive concentrations of glutamate in extracellular space and synaptic clefts can lead to neurotoxic reactions, causing, for example, epileptic seizures [10]. Glutamate is taken up by specific glutamate transporters of which the ones mostly responsible for the uptake process are located in astrocytes. Currently, these transporters are rarely modeled and their reproducibility and replicability can be inconvenient since, based on the research of this work, there are very few simulation codes publicly available.

The purpose of this Master of Science thesis work is to extend the previously published neuron-astrocyte synapse model [11] by incorporating additional biological mechanisms. This neuron-astrocyte synapse model describes the phenomenon of synaptic transmission and plasticity, to which astrocytes have been suggested to take part in. The role of astrocytic mechanisms in this phenomenon is still partly controversial, and requires more studies, which is why it is of interest to continue working with such a synapse model.

The original synapse model is already biophysically and -chemically advanced, setting up a good basis for further development of the model. To reach the purpose of this thesis work, the first aim is to develop a new, biologically realistic component for astrocytic glutamate uptake pathway from the synaptic cleft to the astrocyte. The second aim is to examine whether it is possible to integrate the developed glutamate uptake component into the complex synapse model and simultaneously maintain appropriate model dynamics to ensure that the dynamics of the new synapse model comply with the dynamics of the original model. The third aim is to evaluate the dynamics of the new developed model against the original synapse model dynamics. Lastly, the fourth aim is to perform evaluations also against different conditions, where parameters affecting the rate of the new glutamate uptake component are modified. The first two aims are the most important ones to reach the purpose of this work. In addition, it is of importance to introduce not only the mathematical expressions, but also other implementation details needed to fully reproduce the model.

The neuroscientific background for understanding the basics of neuronal cells and astroglia is presented in Chapter 2. In Chapter 3, the description of the original synapse model, and other materials and methods used to develop and implement the astrocytic glutamate uptake component, are presented. The new glutamate uptake component and the dynamics of the new developed synapse model are introduced in Chapter 4, after which the obtained results are discussed and analysed in more detail in Chapter 5. Chapter 6 concludes this thesis work and its most important results.

2. NEUROSCIENTIFIC AND THEORETICAL BACKGROUND

Computational modeling of neuron-astrocyte interactions and astrocytic glutamate uptake employs a wide range of knowledge from the neuroscience field. In Chapter 2, the basics of neuronal and astrocytes,as well as synapses are presented. The neurobiological focus is on explaining the functionality of cells and synapses and how they contribute to excitability, information processing, synaptic transmission, and formation of synaptic plasticity in the brain. In addition, the neuron-astrocyte interactions, particularly the mechanisms related to glutamate uptake from synaptic cleft to astrocytes, are introduced. Computational modeling of these phenomena is explained, and the most used models for describing neuronal sodium-based excitability and astrocytic calcium-based signaling are presented.

2.1 Neuronal cells

Neurons are one of the most abundant cells in the CNS. Different brain areas contain different neuron types varying in size, shape and morphology, and in physiological properties and functions [1, 12]. However, there are a couple features that are generally detected in all neuronal cells. One is their general structure, consisting of the cell body alias soma, and the neurites [12]. The neurites include dendrites that are the receiving part, and an axon that is the sending part of the neuron [1]. Figure 2.1 presents typical morphologies of a rodent and human pyramidal neurons. A lot of progress has been made in recent years to understand the structure and morphology of neuronal cells in both rodent and human cells *in vivo*. As can be seen from Figure 2.1, the size and morphology of neurons vary between rodents and humans. Since a lot of studies are performed with rodent cells, it is of importance to aim to understand how largely their neuronal function differ from humans [13].

Another feature common for neuronal cells is electrical excitability, characterized as the ability to respond to external stimuli by firing brief voltage pulses called action potentials [17]. The excitability of neurons is covered next.

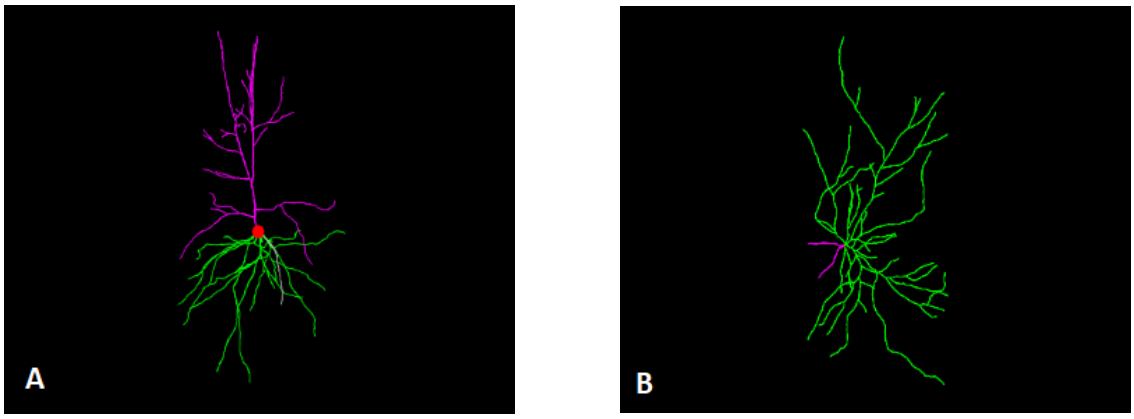

Figure 2.1. *Typical morphology of a cortical pyramidal neuron of A) a human and B) a mouse. The morphologies are from NeuroMorpho.org [14], and originally published in [15] (A) and [16] (B).*

2.1.1 Excitability and neurotransmission

Generally, there are both excitatory and inhibitory neurons [12]. Excitatory neurons release excitatory neurotransmitters, for example glutamate [18]. They fire action potentials to induce an increase in the cell membrane potential of adjacent neurons [1], thus increasing the probability of action potential propagation. Inhibitory neurons release inhibitory neurotransmitters, for example gamma-aminobutyric acid (GABA) [19], and aim to drive the membrane potential of adjacent neurons towards their resting states [1]. In other words, they decrease the possibility of propagation of the action potential. The propagation of action potentials and release of excitatory neurotransmitters have a key role in information transfer from one neuron to another. Thus, in this work, mainly excitatory neurons are covered.

Neurons can connect to each other via synapses to form large neuronal networks. In total, each neuron can form up to 15 000 synaptic connections [20]. Neurons also express special electrophysiological and chemical properties, making them specialized in signal transmission and processing at synapses [1]. Neuron are, for example, able to alter their intrinsic resting membrane potential. The intrinsic resting membrane potential, settling between -40mV and -70mV depending on the neuron type [12], is due to the difference between intracellular and extracellular electric potentials, formed by concentrations of various ions, like potassium (K^+) and sodium (Na^+) ions [1, 21]. The excitability of neurons is characterized by this ability to alter the membrane potential, leading to formation and propagation of action potentials.

Alongside the bioelectrical properties of neurons, release of specific signaling molecules, called neurotransmitters, have a key role in mediating the membrane potential changes [12]. Neurotransmitters released from one neuron bind to the specific receptors ex-

pressed on the membrane of the adjacent, receiving neuron, which then releases its own set of neurotransmitters [22]. The binding of neurotransmitters affects the state of the ligand-gated ion channels in the adjacent neuronal cell membrane. Opening of these ligand-gated ion channels, through which the ions are transported, causes variation in the membrane potential due to the change in extracellular and intracellular ionic concentrations. This variation in the membrane potential is crucial for the excitability and thus for the signaling capabilities of neurons, enabling propagation of action potentials by creating a potential change in the adjacent neurons. The formed interaction of information transfer mediated by transmitter molecules is called neurotransmission, or synaptic transmission (see Section 2.3.1)

2.1.2 Computational modeling of neurons

Thousands of computational models have been developed for neurons. These can vary from models for individual neurons to models for neuronal networks. Although these models vary by composition, they often exploit some of the standardized ways to model neuronal processes, often emphasized on modeling the membrane potential and signal transmission in the synapses. Neuronal processes are typically first expressed by means of mathematical equations and functions, like ordinary differential equations (ODEs), and then implemented with programming languages like Python and MATLAB®. There are also simulation environments for different purposes, such as NEURON simulator [23] for simulating biophysical neurons and neuronal networks, and NEST simulator [24] for simulating spiking neural networks.

One of the first, and perhaps most known, mathematical description of neuronal properties is the Hodgkin-Huxley model (HH-model) for excitability of neurons, describing the propagation of action potentials. The model was presented by Hodgkin and Huxley in 1952 [21, 25]. The data for action potential propagation was obtained from an axon of a giant squid, which was then fitted to the mathematical model. The development of the mathematical model is based on the equivalent electrical circuit of cell membrane, illustrated in Figure 2.2.

The description of electrical equivalent circuit presented below is adapted from [21] and [17]. In Figure 2.2, C_m describes the membrane capacitance, arising mainly due to the dielectric properties of the lipid bilayer. Functionally, the lipid bilayer can be thought as an equivalent to a capacitor. The incoming current (I_m) is divided into capacitive current (I_c), which charges the membrane capacitance, currents for K^+ (I_K) and Na^+ ions (I_{Na}), and the leak current (I_L) passing through the ion channels. The leak current is mainly comprised of the flow of chloride (Cl^-) ions.

Each ion channel has its own resistance, here described as its inverse, conductance. Conductance describes how well the current can flow through its path, here through the

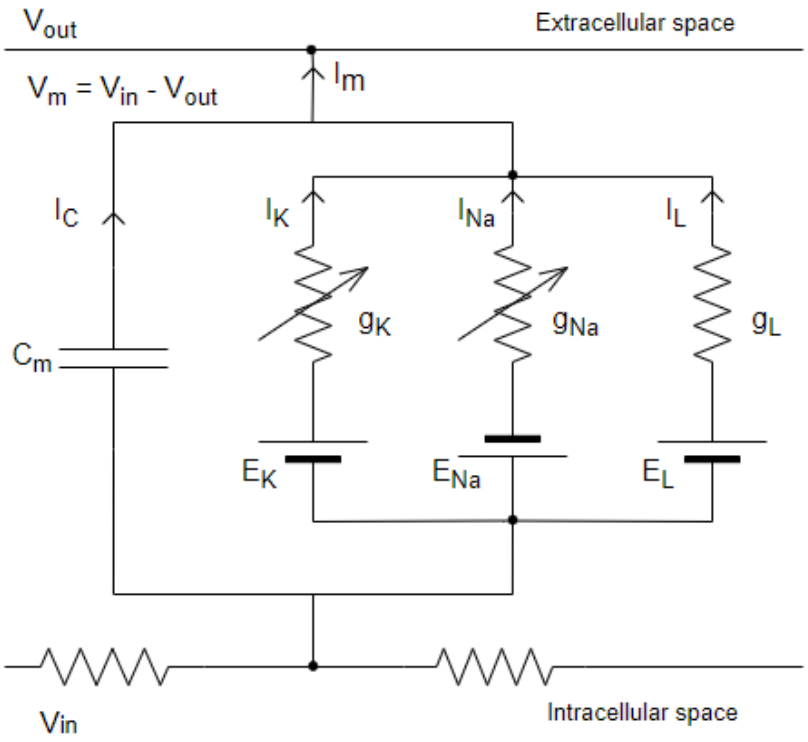

Figure 2.2. *Electrical equivalent circuit of the cell membrane for Hodgkin-Huxley model. Adapted from [21]*

ion channel. The conductances for K^+ and Na^+ channels, and for the leak channel are g_K, g_{Na} and g_L, respectively. The K^+ and Na^+ conductances are independent from each other, but are voltage-dependent, meaning that they are affected by the membrane potential. The leak conductance has a smaller magnitude and is not dependent on the voltage. In this mathematical framework it is assumed to be constant. E_K, E_{Na} and E_L are the equilibrium potentials for K^+, Na^+ and leakage, acting as batteries in the circuit. The difference of each equilibrium potential to the membrane voltage V_m comprises the driving force for each ionic current.

The HH-model is comprised of several basic assumptions and different activation and inactivation states. It is dependent on the currents I_{Na}, I_K and I_L. Each current can be presented with respect to their conductances and driving forces:

$$I_{Na} = g_{Na}(V_m - E_{Na}), \tag{2.1}$$

$$I_K = g_K(V_m - E_K), \tag{2.2}$$

$$I_L = \overline{g}_L(V_m - E_L), \tag{2.3}$$

where g_{Na}, g_K and $\overline{g}_L$ are the Na^+, K^+ and leak conductances, respectively. The overline expression denotes the maximum value. The term $V_m - E_i$ describes the driving force.

The electrical equivalent of the total membrane current can be presented as

$$I = I_c + I_i = C_m \frac{dV_m}{dt} + I_i, \tag{2.4}$$

where I_c is the capacitive current that charges or recharges the membrane capacitance, and I_i is the sum of ionic currents I_{Na}, I_K and I_L. The complete model for all currents that flow across an axonal membrane is presented as

$$\begin{aligned} C_m \frac{dV_m}{dt} = -\overline{g}_{Na} m^3 h (V_m - E_{Na}) - \\ \overline{g}_K n^4 (V_m - E_K) - \overline{g}_L (V_m - E_L) + I. \end{aligned} \tag{2.5}$$

The term $\overline{g}_{Na} m^3 h$ describes the maximum conductance of Na^+, multiplied by specific, numerical values for activation gating variable m and inactivation gating variable h to describe the actual maximum conductance open. Similarly, the term $\overline{g}_K n^4$ describes the maximum conductance of K^+, multiplied by a numerical value for activation gating variable n. Particles m, h, and n are dimensionless numbers between 0 and 1. I is the local circuit current, or injected current. The whole derivation of Equations 2.5 from Equations (2.1), (2.2), (2.3) and (2.4), completed with specific gating variables, can be reviewed from [17] and [21].

The HH-model formalism can be used to describe propagation of action potentials in single-compartment neuron models, but also in multi-compartmental modeling, where the neuron is divided into compartments. In addition to this, a network of neurons can be described by employing multiple neurons [21], each described with the HH-model. Such single-cell and network models have been developed for various types of nerve cells [26]. The HH-model formalism is utilized in the neuronal components of the synapse model [11] that is presented later in this thesis work.

2.2 Glial cells

Another quantitatively and functionally significant cell type in the CNS are non-neuronal glial cells. Glial cells have different specialized subtypes, one of them being astrocytes. Previously astrocytes have been believed to mainly provide structural support for neurons, and act as a “brain glue” [6]. Now, astrocytes are known to have even more fundamental roles in brain functions in health and disease [27]. Astrocytes are, among other roles, known to control the overall homeostasis in the CNS [28]. The homeostasis in the CNS

is a sum of many factors. Homeostatic functions of astrocytes include, for example, controlling over the blood-brain barrier [29], providing metabolic support [6] and participating in synaptic formation and elimination [30]. Astrocytes have also been shown to respond to neural activity and modulating neuronal activity [28, 31]. Recent studies also suggest additional roles for astrocytes, such as involvement in regulation of synaptic transmission [27], neuronal plasticity and learning [6], and memory [32]. However, these roles are still partially controversial, and more experimental studies are needed to show these functions. Even though a great variety of astrocytic functions are known to exist, it is still not fully understood how astrocytes perform these functions.

Figure 2.3 demonstrates a typical protoplasmic astrocyte morphology of a mouse and a human. Typical structural features of astrocytes are soma, and perisynaptic and perivascular processes [33]. The perisynaptic and perivascular processes can be seen in the Figure 2.3 as the branching features, sent out to perform the astrocytic functions. Through the perivascular processes astrocytes can connect to, for example, blood vessels [34]. The perisynaptic processes can also reach up to the neurons at synapses. According to very recent findings, an average astrocyte of a rodent can connect to 12 000 to 120 000 synapses, and an astrocyte of a human up to 2 000 000 [35]. These numbers are rather significant compared to the synaptic connections of neurons.

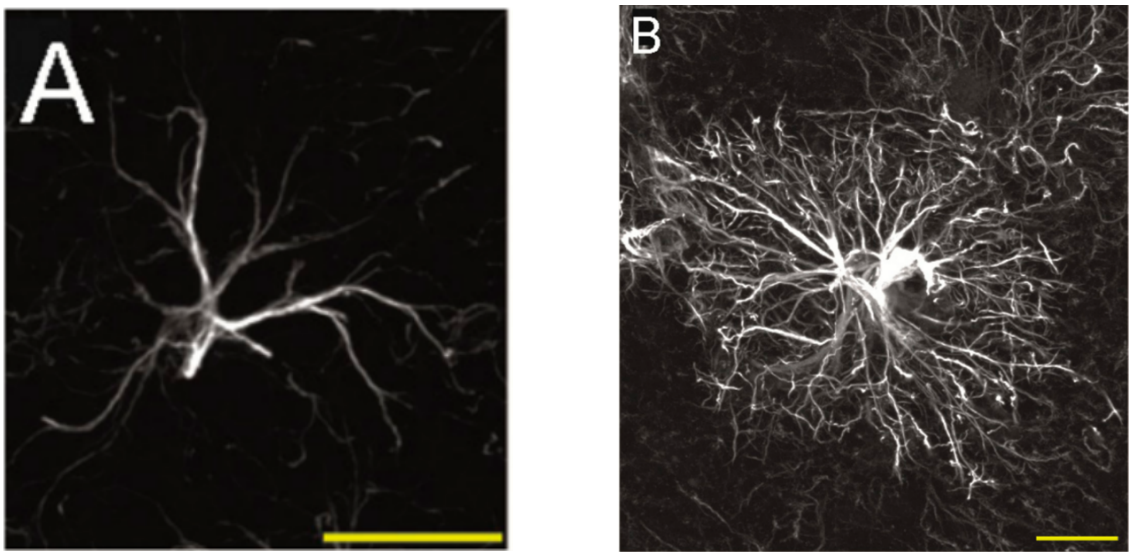

Figure 2.3. *Typical protoplasmic astrocyte morphology from a mouse A) and human B). The figure is taken and modified from [35]. Copyright © 2009 Society for Neuroscience.*

Astrocytes typically have a more negative resting membrane potential compared to the neuronal counterparts, with some exceptions due to the potential ranging from -25mV to -90mV, depending on the brain region [36–38]. The hyperpolarized resting membrane potential is thought to have a critical role for providing the base for the homeostatic functions of astrocytes [39]. Unlike neurons, astrocytes are not able to alter their membrane

potential in the extent required for firing an action potential. Astrocytes do express ion channels for Na^+ ions, which is one key ion for the excitability of neurons. However, astrocytic Na^+ channels have been shown to have a different role than in neurons, and might not be expressed enough in relation to what is required for the formation of action potentials [40]. However, based on current knowledge, astrocytes are not electrically passive cells either, and fluctuations of astrocytic membrane potential have been detected in response to stimuli [41].

Even though astrocytes do not form action potentials, many of their functions are shown to be mediated by intracellular calcium (Ca^{2+}) signaling [42–44], and the changes in the intracellular (Ca^{2+}) concentration can be used to study astrocyte properties. Next, Ca^{2+} excitability in astrocytes, as well as the modeling of Ca^{2+} excitability, are discussed.

2.2.1 Calcium excitability

Studies have revealed that as a response to neuronal activity, astrocytes display increased cytosolic Ca^{2+} oscillation (also called Ca^{2+} spikes, signals, or transients, depending on the literature) [42, 45, 46]. The elevated Ca^{2+} concentration may also propagate as a wave to other adjacent astrocytes [45, 47]. Initially these kinds of findings raised speculation of possible roles of astrocytes in neuronal information processing and transfer. Bazargani and Attwell [42] presented three waves of research evidence in astrocytic Ca^{2+} signaling in their review. The first wave was characterized by the new findings that astrocytes might take part in information processing through Ca^{2+} signaling. *In vitro* studies showed, for example, that increased glutamate concentration led to propagation of intracellular Ca^{2+} signals in the astrocytes, possibly influencing the Ca^{2+} concentration or other mechanism in the adjacent neurons [43, 48]. During the second wave of research, various experimental studies revealed challenges in trying to prove the previous findings of the significance of astrocytic Ca^{2+} signaling. These challenges were partly due to used experimental protocols and animals and due to the lack of suitable pharmacological tools [49]. Lastly, the third wave of research consisted of studies aiming to explain the contradiction between the findings of the first and second waves. It was suggested that astrocytes should also be thought as compartmental structures, expressing different Ca^{2+} transients. To study the possible role of astrocytic Ca^{2+} signaling in synaptic transmission, the Ca^{2+} transients near synapses should be addressed.

The formation of astrocytic Ca^{2+} signaling is also affected by many Ca^{2+}-dependent mechanisms, like activation of inositol triphosphate (IP_3) receptors and mechanisms related to astrocytic glutamate dynamics. Increased intracellular astrocytic glutamate concentrations can also potentially link to increased intracellular Ca^{2+} concentrations of astrocytes [43]. By controlling over the synaptic glutamate concentration, astrocytes can modulate neuronal activity and homeostasis, and it is of future interest to study how the

underlying mechanisms are linked.

Glutamate has an important role in the CNS, but excessive synaptic concentrations of such excitatory neurotransmitter can be inconvenient, as further explained in Sections 2.4.1 and 2.4.3. Even though it is not yet clear if astrocytic glutamate uptake itself is Ca^{2+}-dependent, intracellular Ca^{2+} have been indicated to participate in mediating the glutamate release from astrocytes into the extrasynaptic space [44, 50]. Extrasynaptic glutamate can activate presynaptic neuronal receptors, which then modulates the presynaptic vesicle release probability. Extrasynaptic glutamate can also activate postsynaptic receptors, which may lead to induction of slow inward currents [51]. However, in this thesis work, the extrasynaptic glutamate is only considered to activate presynaptic receptors. The functions of extrasynaptic glutamate observed so far suggest that astrocytic Ca^{2+} signaling could have an effect in synaptic transmission and plasticity [50–52].

2.2.2 Computational modeling of astrocytes

There are currently hundreds of published mathematical models for astrocytes [53]. This number falls significantly behind the amount of neuronal models. As mentioned earlier, astrocytes do not fire action potentials. This is one of the reasons why it has been difficult to gather data for constructing and validating biophysical astrocyte models [54]. For example, imaging of astrocytes can be rather tedious with current imaging methods and might results in poor contrast images. Fortunately, better tools are continuously being developed [54] to catch up with the astrocyte knowledge, and the pace of model releases seems to be rapidly increasing [53]. Fairly many of the astrocyte models still lack more detailed biological properties and are usually very generic, meaning they do not describe the astrocyte functions in some particular brain region or synapse [53].

Like neuronal models, also astrocytic functions are first expressed with mathematical equations and functions, and then implemented with, for example, Python or MATLAB®. The mathematical expressions of astrocytic functions have not yet reached as well-established state as the ones describing neurons (see 2.1.2 and HH-model). However, often some generally known methods are used, such as ODEs, stochastic differential equations (SDEs), and reaction-diffusion modeling. Usually, such implementations contain one or two neurons in addition to the astrocyte and emphasize the neuron-astrocyte interactions. There is also a recently developed tool called ASTRO [55], which can be used to study morphological and functional features of astrocytes.

The modeled entity in astrocyte models is typically astrocytic Ca^{2+} concentration, since Ca^{2+} has a key role in intracellular signaling in many astrocytic functions such as glutamate release [44]. In 1994, Li and Rinzel [56] introduced a model describing Ca^{2+} signaling in cells. Their model has since been widely utilized in astrocyte studies [53]. The model by Li and Rinzel can be applied to model the IP_3-dependent cytosolic Ca^{2+}

signaling in the astrocyte as follows

$$\begin{aligned}\frac{d[Ca^{2+}]_{cyt}}{dt} = (r_{CICR}(\frac{[IP_3]_{cyt}}{[IP_3]_{cyt}+d_1})^3(\frac{[Ca^{2+}]_{cyt}}{[Ca^{2+}]_{cyt}+d_5})^3h^3 + r_{LEAK}) \\ \times([Ca^{2+}]_{free} - (1+c_1)[Ca^{2+}]_{cyt}) \\ -V_{SERCA}\frac{([Ca^{2+}]_{cyt})^2}{([Ca^{2+}]_{cyt})^2 + (K_{SERCA})^2}.\end{aligned} \tag{2.6}$$

The terms r_{CICR} and r_{LEAK} describe the Ca^{2+} induced Ca^{2+} release from the endoplasmic reticulum (ER) to the astrocytic cytosol, and the leak flux from the ER to the cytosol, respectively. $[IP_3]_{cyt}$ is the astrocytic cytosolic IP_3 concentration and $[Ca^{2+}]_{free}$ is the concentration of free Ca^{2+} in the astrocyte. The Ca^{2+} is pumped from the cytosol to the ER with a sarco/ER Ca^{2+}-ATPase pump (SERCA), and this pump flux is described with SERCA-related parameters V_{SERCA} and K_{SERCA}. ATPase is an enzyme that hydrolyzes adenosine triphosphate (ATP) compound. Understanding of the detailed function of SERCA pump is not necessary in this thesis work. Visual representation of these basic components of astrocytic Ca^{2+} signaling can be viewed from Figure 3.1.

Li and Rinzel [56] also described the fraction of active IP_3 receptors, located in the ER of astrocytes as follows

$$\frac{dh}{dt} = \frac{h_\infty - h}{\tau_h}, \tag{2.7}$$

where

$$h_\infty = \frac{Q_2}{Q_2 + [Ca^{2+}]_{cyt}}, \tag{2.8}$$

$$\tau_h = \frac{1}{a_2(Q_2 + [Ca^{2+}_{cyt}])}, \tag{2.9}$$

and

$$Q_2 = d_2\frac{[IP_3]_{cyt} + d_1}{[IP_3]_{cyt} + d_3}. \tag{2.10}$$

The concentration of the intracellular astrocytic IP_3 and the fraction of active IP_3 receptors determine the concentration of cytosolic Ca^{2+} in astrocytes. The parameters a_2, d_1, d_2, d_3, d_5 and c_1 in the Equations (2.6)–(2.10) are obtained from the literature [56] and are not presented in more detail here. The astrocyte component of the synapse model [11],

presented later in this work (Section 3.1.1), employs the modeling of IP_3-dependent Ca^{2+} signaling introduced by Li and Rinzel [56].

Adding expressions to model the glutamate transporters is relatively new. A few published models incorporating glutamate transporters are used as preliminary material for this work and are presented in Section 3.2 in Table 3.1. All of these models included some level of description for the function of astrocytic glutamate transporter.

2.3 Synapses

There are both chemical and electrical synapses, from which chemical synapses have been presumed to be the main mediator of targeted communication in the brain [21]. To simplify, a chemical synapse is a structure that enables a neuron to send information as chemical signal to another neuron or target cell, forming a chain reaction of information propagation. Electrical synapses, also known as gap junctions, are junctions formed by channel proteins, typically connecting dendrite to dendrite or axon to axon [21, 57].

Each neuron can send and receive information. When observing one synaptic connection between two neurons, we can identify a sending, or **presynaptic**, neuron connecting to a receiving, or **postsynaptic**, neuron via the synapse, also referred to as the synaptic cleft [1]. Chemical synapses can be thought as a complex signal transduction device, mediated by neurotransmitters [21, 22]. The postsynaptic response generated through a chemical synapse is due to binding of presynaptically released neurotransmitters (Section 2.1.1).

Gap junctions are called electrical synapses since the presence of such junctions enable electrical coupling and thus electrical pathways between neurons [19]. The information propagates through the channels due to their permeability to ions and other small molecules [57]. These electrical pathways are characterized by low resistance, which helps to prevent loss caused by leakage. Thus, the postsynaptic response is accumulated with only a little attenuation. Astrocytes have also been shown to have gap junctions, which they can in some situations and developmental stages use to form their own networks [6, 58].

Therefore, synapses are special sites that allow cells to connect to each other chemically or electrically. Studying the synaptic level functions reveals information about significant mechanisms occurring in the brain, for example synaptic transmission and plasticity.

2.3.1 Synaptic transmission and plasticity

As learned in Section 2.1.1, synaptic transmission, also called neurotransmission, is characterized by the propagation of neurotransmitter-mediated action potentials. To empha-

size the mechanism in the synaptic level between networks of neurons, the term synaptic transmission is used.

When the presynaptically released neurotransmitters diffuse to the synaptic cleft, they can bind to the receptors on the membrane of postsynaptic neuron [22]. Here, the neurotransmitter of interest is glutamate (Section 2.4.1). Different types of glutamate receptors have been identified in the brain: ionotropic and metabotropic receptors [28, 59]. Ionotropic receptors include N-methyl-D-aspartate receptors (NMDAR), α-amino-3-hydroxy-5-methyl-4-isoxazole propionic acid receptors (AMPAR), and kainate receptors. These are ligand-gated ion channel proteins integrate into the cell membrane. Metabotropic glutamate receptors (mGluRs) are a family of G-protein coupled receptors, whose activation provokes different intracellular G-protein signaling cascades. AMPARs and NMDARs are especially important elements of synaptic transmission and the functioning of neuronal networks.

Neurons play a significant role in synaptic plasticity through synaptic transmission at chemical synapses. Synaptic plasticity means activity-dependent changes in synaptic efficacy and strength [60]. These changes can strengthen or weaken the synapse and last from milliseconds to minutes as **short-term plasticity**, or from tens of minutes to hours, or even a lifetime, as **long-term plasticity** [61]. This thesis work concentrates on the latter.

There are two types of long-term plasticity: long-term depression (LTD) and long-term potentiation (LTP). LTD is characterized as a decrease in synaptic strength, mostly occurring in synapses where glutamate is the primary neurotransmitter [52]. LTP is the opposite process, where the synaptic strength is increased [21]. Decreases and increases in the synaptic strength affect, for example, memory and learning by mediating the synaptic transmission. When the synaptic strength in decreased, the postsynaptic potentials are weakened, descending also the magnitude of neuronal processes, like glutamate release. The effect is opposite when the synaptic strength is increased.

The timing of action potentials (or spikes) is one key function behind the synaptic plasticity. The dependence between action potential timing and synaptic plasticity is called spike-timing-dependent plasticity (STDP) [11]. STDP is an extremely complex phenomenon, which cannot be covered to the full extent in this thesis work. For more comprehensive review of the phenomenon, see [62]. The direction and magnitude of STDP is determined by the order and temporal difference of pre- and postsynaptic action potentials [63, 64]. When the timing of the postsynaptic action potential is before the presynaptic action potential, the temporal difference in negative. Other way around the temporal difference is positive. In some brain areas, the negative temporal difference results in spike-timing-dependent LTD (t-LTD), and the positive temporal difference in spike-timing-dependent LTP (t-LTP). This is demonstrated in Figure 2.4. In this study, the

emphasis is on LTD, and especially on t-LTD.

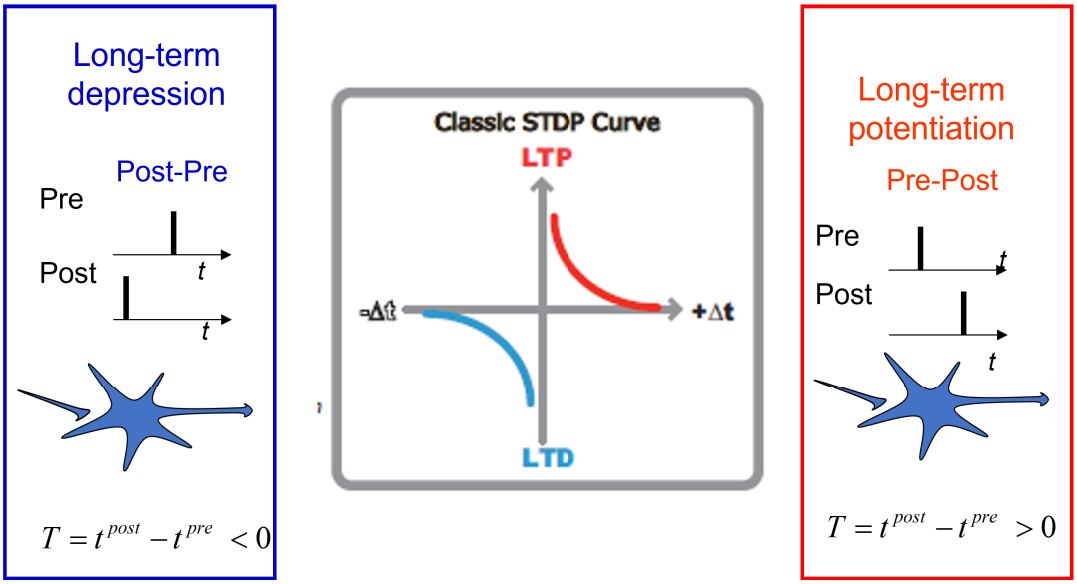

Figure 2.4. *The direction of the spike-timing-dependent plasticity depends on the order and temporal difference of the pre- and postsynaptic action potentials. If the postsynaptic action potential occurs before presynaptic one, the time difference is negative and results in t-LTD in some brain areas. If the presynaptic action potential occurs before postsynaptic one, the time difference is positive and results in t-LTP in some brain areas. In this work, only t-LTD was studied. Courtesy of Prof. Ausra Saudargiene.*

Astrocytes, too, express mechanisms to interact with neurotransmitters like glutamate. Astrocytes have a yet controversial, but suggested role in the synaptic transmission and plasticity. In order to study the role of astrocytic functions, and especially the role of astrocytic glutamate dynamics, it is of interest to better understand the neuron-astrocyte interactions in synaptic plasticity.

2.3.2 Neuron-astrocyte interactions

As learned, neurons and astrocyte express different signaling mechanisms. Neurons are characterized by the ability to fire action potentials, whereas astrocyte signaling is based on the fluctuations in intracellular Ca^{2+} concentrations [17, 42]. Despite the differences in signaling, neurons and astrocytes have been shown to interact with each other bidirectionally in normal brain functions but also in disease. Astrocytes can, for example, send their processes to reach the synapses and may then help to shape the functions of neural networks [58]. Neuron-astrocyte interactions are a complex topic and depend on the cell type, brain area, and developmental stage [65], from which only a small fraction is covered in this work. An example of neuron-astrocyte interactions, characterized by exocytosis and uptake of transmitters and other signaling molecules, during t-LTD induction is given in Materials and Methods (Chapter 3). This interaction is also briefly explained

next.

Neurons can also take up Ca^{2+} ions through ion channels. This influx of Ca^{2+} can lead to multiple different signaling cascades, depending on the phenomenon. Thus, Ca^{2+} is believed to be an important entity in mediating the neuron-astrocyte interactions. For example, combined with the activation of mGluRs, AMPARs and NMDARs, neuronal Ca^{2+} influx can lead to the production of a specific endocannabinoid, 2-arachadonylglycerol (2-AG) in the neuron [7]. Neurons can then release the endocannabinoid 2-AG into the extracellular space, where it can activate cannabinoid receptors on the astrocyte membrane. The binding of endocannabinoids can induce production of another important signaling molecule, IP_3, inside the astrocyte. The increased IP_3 concentration can further affect the astrocytic Ca^{2+} signaling [7], and thus the release of molecules and transmitters, like glutamate, from the astrocyte.

2.3.3 Modeling synapses and neuron-astrocyte interactions

There are a few different general ways to model the information processing at the synaptic level. The simplest way to describe this neuronal connection and synaptic transmission is to consider it as a two-compartmental structure, including the presynaptic and postsynaptic neurons. These neuron models aim mainly to describe propagation of information between neurons, from an action potential at the presynaptic terminal to the response in the postsynaptic terminal. To include also the neuron-astrocyte interaction in synaptic functions, the synapse should be modeled as a tripartite structure [48, 66], consisting of pre- and postsynaptic neurons, and also an astrocyte. The models can be generic, meaning that it does not describe a certain synapse in the brain. For more accurate results, the mathematical expressions can be fitted to describe the functions in a specific, predefined synapse.

There are a range of published models that describe the functions between neurons at synaptic level [67, 68], most of which describe the mechanisms leading to short-term plasticity rather than long-term plasticity. One widely used synapse model is the model introduced by Tsodyks and Markram in 1997 [69, 70]. Their model illustrates the phenomenon of short-term synaptic depression.

In this work, the synapse model by Manninen et al. [11] is utilized. The model is a biophysically detailed synapse model, modified from the model by Tsodyks and Markram, where Ca^{2+}- and IP_3-dependent astrocyte regulates the synaptic functions at the layer 4 to layer 2/3 cortical synapse. The model describes the mechanisms leading to long-term depression, t-LTD. This model seems to hold the place for most biophysical synapse models describing t-LTD for this specific synaptic connection. To participate in the development of non-generic models, it was of interest to continue working on this particular model.

2.4 Glutamate uptake

Glutamate uptake is a process where excess neurotransmitter glutamate is taken up from the synaptic cleft and extrasynaptic space. The mechanism relies on cellular uptake through specific glutamate transporters. Glutamate uptake supports the recycling of glutamate for neurotransmitter release, but it can also be metabolized for other cellular functions.

2.4.1 Neurotransmitter glutamate

Glutamate is a free amino acid and also a major excitatory neurotransmitter in the CNS [18], responsible for a large part of excitatory synaptic transmission [65]. Depending on the brain area, there is approximately 5-15 mmol of glutamate per kilogram on wet weight [18]. Typically, the blood-brain-barrier is impermeable to glutamate [9], so the glutamate required for brain functions must be metabolized and recycled in the brain itself.

After a presynaptic neuron receives a stimulus, it can release neurotransmitter glutamate into the synaptic cleft from specific structures called presynaptic vesicles. From the cleft, glutamate can bind to glutamate receptors in neurons and glial cells to carry out its role in normal brain functions. The normal synaptic glutamate concentration lies in the scales of µM to nM [71, 72]. The measured value depends partly on the brain area and also on the practical measurement system.

Glutamate is a vital signaling molecule, yet excessive concentration of such excitatory neurotransmitter in the synaptic cleft may cause over-stimulation of neuronal glutamate receptors [73]. Excess activation of glutamate receptors in neurons is potentially neurotoxic [74, 75] and can cause for example epileptic seizures [10], and possible neuronal cell death [76].

There has not been detected any significant level of extracellular enzymatic glutamate degradation, so the residual glutamate must be cleared from the synaptic cleft cellularly, through specific glutamate transporters, [18] by a process called glutamate uptake. When looking at the pathway of glutamate released from the presynaptic neuron, astrocytic glutamate uptake is a mechanism under a regulatory pathway called glutamate-glutamine cycle (Section 2.4.3).

2.4.2 Glutamate transporters

Astrocytes and neurons express different types of glutamate transporters, through which glutamate is taken up into the cell. Here we discuss about the high-affinity glutamate transporters called excitatory amino acid transporters, or EAATs [59] [77]. In this transporter family, there are five EAAT proteins named EAAT1 (GLAST), EAAT2 (GLT-1),

EAAT3 (EAAC1), EAAT4 (EAAT4) and EAAT5 (EAAT5) [78, 79]. The names in the parentheses are the corresponding transporter names in rodents.

EAAT3, EAAT4 and EAAT5 are only expressed in neurons [80–82], whereas astrocytes express glutamate transporters EAAT1 and EAAT2 [59, 83]. However, it has been observed that 5-10% of the EAAT2 protein is also found in neurons [18].

Studies have revealed that the roles of EAAT4 and EAAT5 in glutamate uptake is insignificant, and their function is concentrated in other tasks [18]. In addition, Holmseth et al. [80] suggested that EAAT3 is 100-fold less abundant than EAAT2 in young adult rat hippocampus and is less involved in neurotransmission. Current knowledge does suggest that EAATs in astrocytes (EAAT1 and EAAT2) would be responsible of about 80-90% of glutamate uptake in the whole brain [22, 75], suggesting that neurons are significantly less active in clearing the extracellular and synaptic glutamate.

Holmseth et al. [80] also suggested that about 95% of glutamate uptake in hippocampus is through EAAT2, probably due to a higher transport activity. Based on this, EAAT2 can be speculated to be the main transporter responsible of the uptake of synaptically-released glutamate [75, 77], albeit similar data from other brain areas is still needed. This, however, supports the finding that most of the glutamate transporter models have incorporated a component specifically for EAAT2.

Glutamate transport through EAATs is coupled to intake of three Na^+ ions and one hydrogen (H^+) ion, and outward of one K^+ ion [78, 84]. Glutamate uptake also consumes 1 ATP molecule per glutamate molecule, making it highly energy-consuming process. ATP and the ion transport are used as the driving force and energy source to transport glutamate. [73].

2.4.3 Cellular uptake of glutamate

There is no biological mechanism to convert or metabolize glutamate extracellularly, so in order to maintain healthy glutamate concentration, the brain must have high and rapid activity of glutamate uptake [59, 75]. Glutamate uptake by the cells provides long-term maintenance of extracellular glutamate levels. Since astrocytes are believed to be the primary cells responsible for glutamate uptake, this work mainly concentrates on explaining glutamate uptake by astrocytes.

Glutamate receptors are found widely in the brain, for example in astrocytes, dendrites, nerve terminals, and neuronal cell bodies [59]. This means, that the process of glutamate uptake must remove glutamate not only form synaptic cleft but also extrasynaptically, meaning outside the synapse. In this work, the main emphasis is on the glutamate uptake from synaptic cleft, albeit extrasynaptic glutamate uptake is also covered in the model. In homeostasis extracellular glutamate concentration ranges in the nM–µM scale, whereas

intracellular astrocytic glutamate concentration lies in mM range [75, 85]. Thus, glutamate is taken up into the cell against its concentration gradient: this explains the high demand of energy needed for glutamate transport [75].

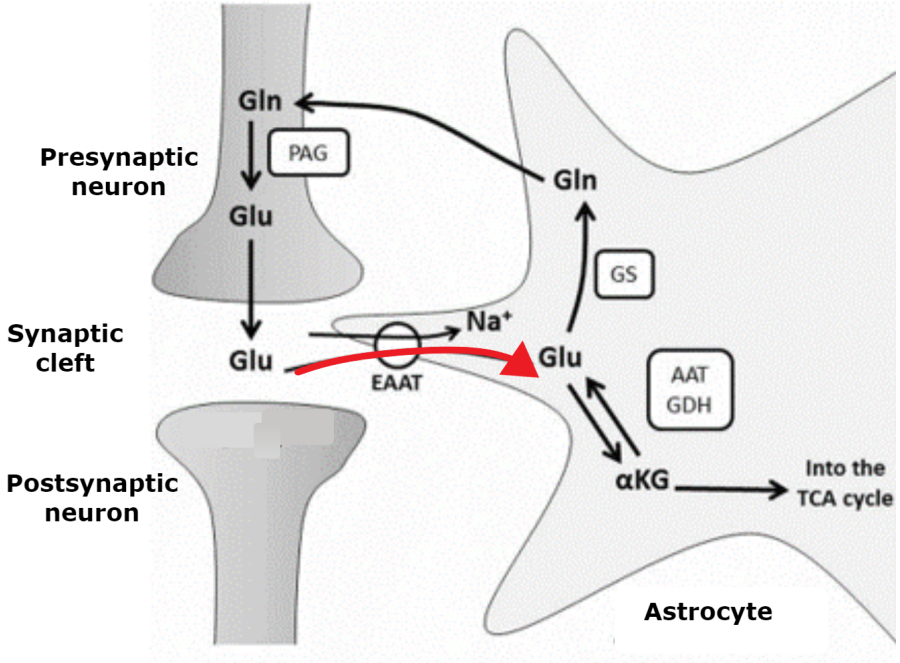

Figure 2.5. *Simplified illustration of glutamate-glutamine cycle between the neurons and astrocyte. The astrocytic glutamate uptake pathway is highlighted in red. Figure is modified from [86].*

Glutamate is released into the synaptic cleft from the presynaptic neurons. This increases the temporal glutamate concentration at the synapse, provoking cellular glutamate uptake. As explained earlier, glutamate can bind to the receptors on the membrane of adjacent postsynaptic neurons. It can, however, also diffuse back from the synaptic cleft and activate also the receptors of the presynaptic neurons and thus affect its own release. This can be called the spillover of glutamate [87]. Even with the spillover of glutamate, the amount of released glutamate exceeds the concentration needed for activating the postsynaptic receptors. Astrocytes actively observe the glutamate dynamics in the synapse and control the glutamate levels by taking excess glutamate into the cell through EAATs (see Section 2.4.2). Inside the astrocyte, glutamate can be converted into glutamine which does not possess such excitatory properties as glutamate [59, 88]. Glutamine is safe to be released from the astrocyte and to be transported back to the presynaptic neuron. Once inside the presynaptic neuron, glutamine can be converted back to glutamate. However, not all transmitter glutamate in astrocytes is converted into glutamine, and it can be used, for example, for metabolic purposes [59], or be released in the form on glutamate from the astrocyte to the extrasynaptic space. Transmitter glutamate in the extrasynaptic space can activate presynaptic receptors, for example, NMDARs. Activation of presynaptic NMDARs can provoke, for example, activation of a specific protein phos-

phatase called calcineurin (CaN), which participates in the release probability of the next set of presynaptically released glutamate [11].

The whole recycling process – from release of glutamate from presynaptic neuron, uptake of glutamate into astrocytes, metabolizing glutamate to glutamine, and then transporting it back to presynaptic neurons to be re-used as glutamate neurotransmitter – is called glutamate-glutamine cycle [59, 86]. In this thesis work, the glutamate uptake from the synaptic cleft into astrocyte is emphasized. The illustration of the glutamate-glutamine cycle is presented in Figure 2.5, in which the astrocytic glutamate uptake pathway is highlighted in red.

The regulation of astrocyte-mediated glutamate concentration seems to have a crucial role in the bigger picture. Thus, it has been suggested that astrocytes may indeed affect some neuronal functions, like synaptic transmission and plasticity [27, 32], especially in some brain areas, for example somatosensory cortex [7].

2.4.4 Computational modeling of glutamate uptake

Modeling glutamate transporters is a relatively novel topic in the field of neuroscience. More data is needed to reach a more biophysical way for modeling these transporters. In this work, a detailed survey of glutamate transporters models was performed to form a comprehensive overview of the current situation of modeling glutamate transporters.

As presented earlier, out of all high-affinity glutamate transporters, EAAT2 is thought to have the biggest role in glutamate uptake to astrocytes. Even though quite a few different modeling approaches were found as a result of the survey, they mostly relied on this piece of knowledge, and described the transporter as EAAT2. As the goal of this work was to develop a new glutamate transporter model, more information about modeling these transporters is presented in Chapter 3.

3. MATERIALS AND METHODS

In this chapter, the materials and methods used to perform the model development are introduced. The presented materials were reviewed carefully over several months, in order to gather understanding of a suitable level of complexity and the best model for the astrocytic glutamate uptake pathway.

In general, there are two different levels of modeling: biophysical and phenomenological. In more biophysical models, there are also some extent of biologically complex features and mechanisms included. On the other hand, phenomenological models leave out the complex biological features. There are, certainly, also models that lay in between these two levels. The aim of this work is to integrate a new component, describing the astrocytic glutamate uptake pathway from the synaptic cleft, into a previously published model of a synapse [11]. To meet the aims of the work, it was not necessary to use the most complex biophysical glutamate transporter model. A simpler, intermediately phenomenological approach was chosen also due to computational limitations.

3.1 Computational synapse model

Manninen et al. [11] presented a new somatosensory cortical layer 4 to layer 2/3 neuron-astrocyte synapse model, describing the synapse as a tripartite structure, containing an axonal compartment of a presynaptic neuron, dendritic and somatic compartments of a postsynaptic neuron, and a nearby fine astrocyte process. From now on the model is referred to as the synapse model.

The aim of the synapse model is to increase understanding on how astrocytes affect t-LTD, and how this astrocyte-mediated t-LTD affects synaptic properties in the developing somatosensory cortex [11]. Since glutamate dynamics affect the astrocytic processes, it is of interest to study how the variation in the astrocytic glutamate pathway affects t-LTD. The original synapse model, however, did not model the effects of glutamate uptake from synaptic cleft to the astrocyte.

The aim of this thesis work is to create a new component to the model, describing the glutamate uptake pathway from synaptic cleft into the astrocyte. This allows studying the effects of possible impairments in the astrocytic glutamate dynamics. In this section, the

synapse model is explained in such extent that the reader is able to understand its equations and components that were modified to implement the new properties of glutamate uptake.

3.1.1 Model description

As mentioned earlier, the synapse model is comprised of three distinct components (pre- and postsynaptic neurons and an astrocyte). The function of each component is constructed with mathematical equations, and were then carefully validated against experimental data. The visual composition of the model, including all the mechanisms and signaling molecules that were originally modeled, is shown in the illustration in Figure 3.1.

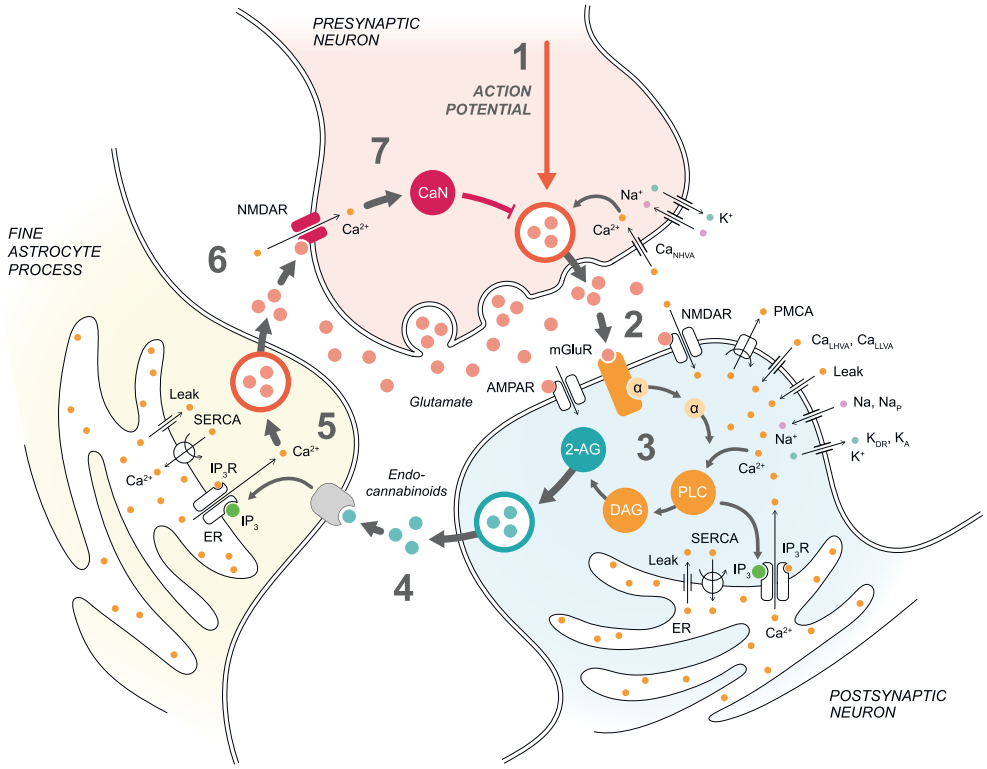

Figure 3.1. *Graphical illustration of the tripartite neuron-astrocyte synapse model, originally published in [11].*

In the initial work [11], the pre- and postsynaptic channels and ionic currents are described according to previously published neuronal formalism, such as the HH-model (see Chapter 2.1.2 for the description of HH-model). Pre- and postsynaptic neurons carry neurotransmission by firing action potentials and responding to the released neurotransmitter glutamate and other signaling molecules, thus are responsible for the propagation of information. The astrocyte component is Ca^{2+}- and IP_3-dependent, and is based on previous models, such as the model by Li and Rinzel [56]. In practise, the release of glutamate from the astrocyte occurs only when the astrocytic Ca^{+} concentration exceeds a

threshold level of 0.3 µM. Together with Ca^{2+}, IP_3 regulates intracellular astrocyte events in the synapse model.

Even though the synapse model does not include a direct pathway for astrocytic glutamate uptake from synaptic cleft, the model included all the key mechanisms that were required to computationally describe synaptic t-LTD in developing somatosensory cortex. The correct glutamate concentrations in different compartments are controlled with computational and mathematical simplifications to produce biologically realistic outcome. The original glutamate and other signaling dynamics can be view from the illustration in Figure 3.1. The glutamate cycle begins with vesicular glutamate release from the presynaptic neuron to synaptic cleft due to an action potential (1). The glutamate released to the synaptic cleft activates presynaptic NMDARs, and postsynaptic mGluRs, NMDARs and AMPARs (2), but due to absence of glutamate transporters, it does not directly activate astrocytic processes. The activation of postsynaptic mGluRs and NMDARs together with an influx of Ca^{2+} then activates a G-protein coupled signaling cascade which eventually leads to a production of endocannabinoid 2-AG (3). 2-AG is then released from the postsynaptic neuron, after which it can bind to the nearby astrocyte (4). The binding of this endocannabinoid triggers Ca^{2+} signaling in the astrocyte, leading to an increase in the astrocytic Ca^{2+} concentration. This triggers the exocytosis of glutamate from the astrocyte to the extrasynaptic space (5). The released glutamate is then again able to activate presynaptic NMDARs (6) in order to provoke activation of CaN and modify the release probability of a new release cycle of presynaptic glutamate (7).

The direction and magnitude of long-term plasticity in the CNS is dependent on the temporal difference of the occurance of pre- and postsynaptic action potentials. In order to simulate the t-LTD, negative temporal differences (ΔT) between -10 ms and -200 ms, with step size of 10 ms, were used [11]. The negative sign means that the postsynaptic stimulus occurred before the presynaptic stimulus. The whole t-LTD stimulation protocols consisted of the t-LTD induction protocol itself, and also protocols before and after t-LTD induction. The stimulation protocols are demonstrated with two pulses in Figure 3.2. The protocol before t-LTD induction (A) is performed as five presynaptic pulses at 0.2 Hz, from which Figure 3.2A presents the first two. The t-LTD induction (B) included 100 post-pre pairings at the same frequency of 0.2 Hz, of which Figure 3.2B presents two pairings. The post-pre pairings describe the situation where the postsynaptic neuron is stimulated before presynaptic neuron, and they were performed for each temporal difference (from -10 ms to -200 ms). Similarly to the protocol before, also the protocol after t-LTD induction (C) is performed with 5 presynaptic pulses at frequency of 0.2 Hz, of which two are presented in Figure 3.2C.

The published article [11] and this thesis work graphically demonstrate only specific temporal differences of ΔT = -10 ms, ΔT = -50 ms, ΔT = -100 ms, ΔT = -150 ms and ΔT = -200 ms. The reason for this decision is to be able to describe as large as possible

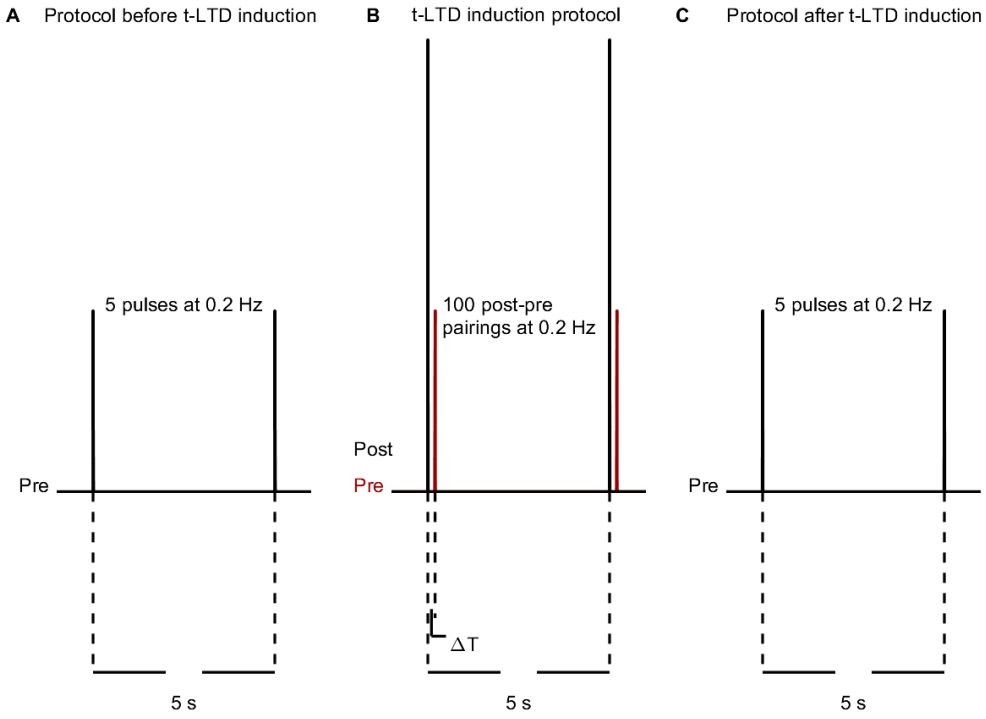

Figure 3.2. *The t-LTD induction stimulation protocol, adapted from [11]. The protocol consisted of before t-LTD induction as five presynaptic pulses at 0.2 Hz (A); t-LTD induction as 100 post-pre pairings at 0.2 Hz (B); and after t-LTD induction as five presynaptic pulses at 0.2 Hz (C).*

range of the temporal differences within the limit of computational power. This decision does not affect the obtained results.

Manninen et al. [11] were able to show the following experimental findings with their synapse model. Firstly, they showed the dependence of t-LTD on the temporal difference between pre- and postsynaptic action potentials, by confirming that different temporal values produced different magnitudes of t-LTD. The results also show that astrocytes take part in inducing and maintaining t-LTD through Ca^{2+} signaling and glutamate exocytosis. Ca^{2+} signaling was found to be affected by postsynaptic 2-AG release. Lastly, the presynaptic neuron detected the glutamate released from astrocyte. This was shown to affect the presynaptic vesicular release probability, and thus affecting t-LTD.

3.1.2 Model equations

Here, the original equations relevant for understanding this thesis work are presented. All the equations and parameter values are from the model by [11]. The original model codes are available in *ModelDB* [26]. The model consist of five separate python files: `preneuron.py`, `postneuron.py`, `astrocyte.py`, `run_pairings.py` and `run_before_and_after_pairings.py`. The first three files contain the equations and

parameters needed to describe the function of the pre- and postsynaptic neurons and the astrocyte. The two latter files contain the protocols for simulating the t-LTD induction.

When the presynaptic neuron is stimulated, it releases glutamate to the synaptic cleft. The synapse model presents a 10 % spillover of glutamate, meaning the fraction of the synaptically released glutamate that binds to the presynaptic NMDARs. Thus, technically, 90 % of the presynaptically released glutamate diffuses to the synaptic cleft and is free to bind on the postsynaptic receptors or to be taken up by transporters. As mentioned, no such transporters are modeled yet. However, in the initial synapse model, there is a consumption of glutamate, imitating the amount of glutamate taken up from the synaptic cleft due to postsynaptic neuronal glutamate uptake. This glutamate consumption was included to realistically describe the glutamate dynamics in the synaptic cleft, even though it did affect the intracellular state of the postsynaptic neuron. The reaction rate for this glutamate consumption is described as

$$v_{Glu,f,post} = k_{Glu,f,post} \cdot (1 - f_{Glu,pre}) \cdot [Glu]_{syncleft} \tag{3.1}$$

where $k_{f,Glu,post}$ ($\frac{1}{ms}$) is the rate constant for the glutamate consumption, $f_{Glu,pre}$ is the fraction of spillover going to the presynaptic NMDAR and $[Glu]_{syncleft}$ (μM) is the current concentration of glutamate in the synaptic cleft.

The synaptically released glutamate can also bind and unbind to the postsynaptic mGluRs, and activate a current through postsynaptic NMDARs and AMPARs. The expressions for the function of the two latter receptors were not modified for this implementation, and thus are not presented here. The reaction rate for glutamate binding to postsynaptic mGluR is described as

$$v_{mGluR,f,post} = k_{mGluR,f,post} \cdot (1 - f_{Glu,pre}) \cdot [Glu]_{syncleft} \cdot [mGluR]_{post} \tag{3.2}$$

where $k_{mGluR,f,post}$ ($\frac{1}{\mu ms}$) is the rate constant for glutamate binding to mGluR, and $[mGluR]_{post}$ (μM) is the concentration of postsynaptic mGluR. After glutamate has bound to the mGluR, they form a complex called $[Glu\_mGluR]_{post}$.

Some of the glutamate can also unbind and be released back to the synaptic cleft. Reaction rate of glutamate unbinding to mGluR is then described as follows

$$v_{mGluR,b,post} = k_{mGluR,b,post} \cdot [Glu\_mGluR]_{post} \tag{3.3}$$

where $k_{mGluR,b,post}$ ($\frac{1}{ms}$) is the rate constant of glutamate unbinding, and $[Glu\_mGluR]_{post}$ (μM) is concentration of postynaptic glutamate-mGluR complex formed after binding of glutamate.

As a result of the presynaptic glutamate release, and the glutamate binding and unbinding to postsynaptic mGluR, the concentration in the synaptic cleft changes as follows

$$\frac{d[Glu]_{syncleft}}{dt} = v_{Glu,f,post} - v_{mGluR,f,post} + v_{mGluR,b,post} + \sum_j \frac{G_{pre}N_{pre}P_{rel,pre}R_{rel,pre}}{k_{Glu,pre}N_A V_{syncleft}}\delta(t-\tau_j). \tag{3.4}$$

The term $\sum_j \frac{G_{pre}N_{pre}P_{rel,pre}R_{rel,pre}}{k_{Glu,pre}N_A V_{syncleft}}\delta(t-t_j)$ describes the presynaptic glutamate release dynamics and the actual amount of glutamate released to the synaptic cleft during time points depending on action potentials and Ca^{2+} concentration; G_{pre} is the number of glutamate per presynaptic vesicles; N_{pre} is the number of readily releasable presynaptic vesicles; $P_{rel,pre}$ is the release probability of presynaptic glutamate vesicle; $R_{rel,pre}$ is the fraction of releasable presynaptic glutamate vesicles; $k_{Glu,pre}$ is a scaling factor to convert concentration from M to µM; N_A is Avogadro's constant; $V_{syncleft}$ (l) is the volume of synaptic cleft and $t = \tau_j$ describes the time point when glutamate release occurs. The (Dirac's) delta function, described as δ, has unit of $\frac{1}{ms}$.

The synapse model also presents the expression of glutamate dynamics in the extrasynaptic space between the astrocyte and presynaptic neuron. The glutamate concentration in the extrasynaptic space is dependent on the astrocytic glutamate uptake and release, as following

$$\frac{d[Glu]_{extsyn}}{dt} = -r_{astro}[Glu]_{extsyn} + \sum_i r_{vesext,astro}G_{astro}N_{astro}P_{rel,astro}R_{rel,astro}\delta(t-\tau_i). \tag{3.5}$$

In Equation (3.5) $r_{astro}[Glu]_{extsyn}$ describes the astrocytic glutamate uptake from the extrasynaptic space, r_{astro} being the clearance rate of glutamate. The summation term $\sum_i r_{vesext,astro}G_{astro}N_{astro}P_{rel,astro}R_{rel,astro}\delta(t-\tau_i)$ presents the astrocytic glutamate release dynamics, and the actual concentration of glutamate released to the extrasynaptic space; $r_{vesext,astro}$ is the ratio between volumes of astrocytic vesicle pool and extrasynaptic space; G_{astro} is the glutamate concentration per one pool of astrocytic vesicles; N_{astro} is the number of readily releasable astrocytic pools; $P_{rel,astro}$ is the release probability of the glutamate; $R_{rel,astro}$ is the fraction of releasable astrocytic vesicle pools.

3.2 Computational glutamate transporter models

A comprehensive search was performed to create understanding of the level and methods for describing glutamate uptake by glutamate transporters. Both computational and theoretical models including glutamate uptake were found, preferring the ones implemented in astrocytes. A total of 43 models were found, from which 42 were computational and one was a purely theoretical implementation. Furthermore, 40 of these models presented glutamate uptake in astrocyte, and two with glutamate transporter located in other cells.

Each of the 43 models were studied separately, paying attention particularly to how the glutamate transporter was modeled. Several months were reserved for this part of the thesis work, since thorough familiarization with glutamate transporter models increased the significance of this thesis work for future modeling perspectives. To assess which models would pass this preliminary evaluation, they were evaluated against the perceived capability of integrating the modeling approach of glutamate transporter to the synapse model. Thus, if the function of glutamate transporter was dependent on a variety of model-specific functions, it most likely could not be used in this work. Also, if the astrocytic glutamate uptake was merely a side note, the model was not included in further evaluations. Most of the reviewed models were discovered not suitable for the frame of this work.

Out from the 42 computational models, simulation codes were available for only 7 models, which bolsters the need for improving the reproducibility and replicability of the astrocytic modeling field. Fortunately, the bulk of the publications presented the underlying glutamate uptake equations clearly enough to be referred and evaluated. However, without detailed information of the implemented simulation codes, the simulation results of the models probably could not be reproduced identically.

Not all of the 43 models are referenced in this thesis, but the few models estimated suitable for further examination in the scope of this work are presented in Table 3.1. All the described models represent different ways to model astrocytic glutamate uptake, which suggests that there is not yet one general way to describe the process. Most of these models either directly stated that they employ the transporter EAAT2, or referred to its characteristics even though not stating directly the type of the glutamate transporter they modeled. When studying these models, the main emphasis was in the following criteria:

1. How is the astrocytic glutamate uptake modeled?
2. What is the level of complexity in the model?
3. What is the aim of the study?
4. What are the main results of the study and was the work successful?

The idea was to choose models where the astrocytic glutamate uptake component could be separated and re-implemented into a completely different model. Thus, it could not

be too biophysical and complex to begin with, which then connects to the criteria number 2. There were a few credible models, and to decide between these, also the aims and the main results were sieved through. In optimal situation, the aim of the study would also be related to STDP or similar phenomena. Lastly, the results were reviewed to check whether the study was reliable and successful.

After a thorough study of the models, presented in Table 3.1, it was concluded that the best outcome would be obtained not by implementing one already existing glutamate uptake model but to take parts of one or more models and using them as a base to create a component for glutamate dynamics that fits the synapse model. In this work, the glutamate uptake models from Tewari and Majumdar [90] and Blanchard et al. [93] were used as an inspiration.

The model by Tewari and Majumdar [90] was selected due to its mechanism for describing glutamate dynamics in the synaptic cleft: the implementation was rather independent and also quite simple. The approach has some resemblance to the ones used in the synapse model. In addition, the model was used to study LTP in hippocampus, so the approach could be assumed to be suitable for studying STDP in the CNS. The results from [90] address the success of the study, and the equation presented for synaptic glutamate dynamics was detected to be used also in later studies.

In [90], astrocytic glutamate uptake was described by a simple uptake rate. The astrocytic glutamate uptake was dependent on the glutamate concentration in the synaptic cleft. The rate of the uptake then affected the glutamate dynamics in the synaptic cleft as follows

$$\frac{dg}{dt} = n_v \cdot g_v \cdot E - g_c \cdot g, \tag{3.6}$$

where g is the glutamate concentration in the synaptic cleft, n_v is the number of docked vesicles, g_v is the glutamate concentration in synaptic vesicles, E is the effective fraction of vesicles in the synaptic cleft, and g_c ($\frac{1}{ms}$) is the uptake rate of glutamate from the synaptic cleft into the astrocyte. Thus, the effect of astrocytic glutamate uptake affected the glutamate dynamics in the synaptic cleft as a clearance rate.

The model by Blanchard et al. [93] was selected due to the rather incomplicated mechanism to model intracellular glutamate concentration in the astrocyte. It was also found to be easily adapted to fit the synapse model. The intracellular astrocytic glutamate concentration was described as follows

$$\frac{dGlu_A}{dt} = Glu_{E\rightarrow A}(t) - V_{gme}. \tag{3.7}$$

In the Equation (3.7), $Glu_{E\rightarrow A}(t)$ denotes the transport of glutamate from extracellular space to the astrocyte with respect to time, and V_{gme} denotes the astrocytic glutamate

Table 3.1. *Summary of the notable computational models with glutamate uptake components for this thesis work.*

Authors	**Glu uptake equations**	**Description**
Silchenko and Tass 2007 [89]	6	Silchenko and Tass aimed to model the influence of astrocytic glutamate release on the paroxysmal depolarization shifts (PDS) in neurons. They also modeled the glutamate uptake by astrocytes, and eventually combined it with the release rate in order to achieve the equation for the extrasynaptic glutamate concentration.
Tewari and Majumdar 2012 [90]	1	Tewari and Majumdar aimed to present a comprehensive synapse model to mathematically describe the experimental work of astrocyte modulated NMDAR-independent LTP in hippocampus by Perea and Araque [91]. They simulated information processing both for astrocyte-independent and astrocyte-dependent pathways.
Allam et al. 2012 [92]	6	Allam et al. modeled the kinetics of the glutamate transporter in astrocyte. The aim was to study the role of astrocytic glutamate uptake on synaptic responses and neuronal spiking. Unfortunately they did not state proper reasoning for their biologically significant choices in their equations.
Blanchard et al. 2016 [93]	1	Blanchard et al. modeled neuro-glio-vascular coupling to study the relationship between local neuronal activity in epileptiform event, and changes in the cerebral blood flow. The observations included contribution of astrocytic glutamate uptake.
Li et al. 2016 [94]	2	Li et al. described the astrocytic glutamate dynamics by taking into account also the equilibrium concentration and the effect of astrocytic Ca^{2+} concentration. The glutamate concentration change was modeled for specific time constant. The aim was to study how astrocytic glutamate uptake rate affected epileptic seizure dynamics.
Conte et al. 2017 [95]	1	Conte et al. modeled the properties of a glutamate transporter by its reversal potential and current. The reversal of the transporter was used to explore the mechanisms of recurring spreading depolarization.
Flanagan et al. 2018 [96]	5	Flanagan et al. modeled the influence of astrocytic glutamate and EAAT2 activity on post-synaptic neuronal excitability. The model estimated the changes in synaptic glutamate concentration with respect to the glutamate removal rate by EAAT2. They also aimed to describe glutamate clearance.
Kalia et al. 2021 [97]	2	Kalia et al. presented a model that aimed to study bulk ion species (Na^+, K^+, Cl^-) and their reaction when Na^+/K^+-ATPase (NKA) is switched off. Glutamate and Ca^{2+} dynamics are reported, but they are not discussed in more detail, which favored the opinion to not use this model.

consumption. Astrocytic glutamate consumption can include different intracellular mechanisms, for example metabolizing or release of glutamate. In the original synapse model and this thesis work, the astrocytic glutamate consumption, (3.7), is described only as the release of glutamate from the astrocyte. Thus, the intracellular glutamate concentration is dependent of all the in-taken glutamate from extrasynaptic space, and of the glutamate being released from the astrocyte.

3.3 Developing the new model

The model development was performed by combining the approaches from the original synapse model, explained in Section 3.1, and the model equations and approaches described in Section 3.2. The new implementation required also some new parameters, which were then fitted against the model performance. The resulting implementation is presented in the results, in Section 4.1.

The model development was performed keeping in mind the biological aspect of the work. The new implementation and variables were to be realistic and justified with previous knowledge. Due to the complexity of the original synapse model, this phase of the thesis work required extensive understanding of many signaling cascades of the model, and thus the function of all five code files.

3.4 Simulations

This section describes the simulation plans for testing the robustness of the new implementation and for studying the role of glutamate uptake. The model implementation was performed in Python, and the data analysis was executed with MATLAB.

Each simulation was performed by executing the two Python files, `run_pairings.py` and `run_before_and_after_pairings.py` in terminal. The total time spend for each simulation varied from 1.5 hours to 6 hours, depending on the number of temporal differences included. The computer used for these simulations had 32 GB installed RAM and Intel(R) Core(TM) i7-8650C processor.

3.4.1 Evaluating the new model implementation

The main goal of the work was to develop a new implementation for the synapse model, where the direct pathway for astrocytic glutamate uptake would be considered. After the required modifications were made, extensive simulations for testing the functionality of the implementation were performed.

When the new implementation was proven to be working without errors, the output of the model was needed to be optimized. The goal was to achieve similar dynamics as with

the original model, as this would indicate that the modifications did not interfere with the fundamental properties of the model. Various simulations were performed in order to fit one parameter at the time, and to stay alert whether the performed modification caused unwanted output on other parts of the model.

In this phase, the equations, ratios and parameters were to be considered and tested carefully. Modification were done one-by-one with minimal changes at a time. This was necessary, because even small changes led to rather large-scale effects in the reaction rates and dynamics in such biophysically detailed model. This phase was evaluated graphically, by plotting the model outputs for both the original and the new implementation.

3.4.2 Evaluating the functionality of the new model dynamics

After conforming appropriate level of dynamics of the new implementation, further testing was performed. The functionality of the implementation was tested by simulating three different conditions that could be biologically realistic in impaired brain functions: (1) astrocytic glutamate uptake rate is increased, (2) astrocytic glutamate uptake rate is decreased, and (3) astrocytic glutamate uptake is completely blocked.

These additional test simulations changed the set-up of the original model, by emphasizing the effect of changes in the astrocytic glutamate uptake. The tests also helped to further study and analyze the model, enabling to evaluate whether its dynamics were realistic or justifiable after changing the optimized expression. Simulating these three conditions allowed also tentatively study the effect of the rate of the astrocytic glutamate uptake to t-LTD, however more experimental data is required to comprehensively validate the model.

4. RESULTS

The main result of this thesis work is the description of the new, developed computational model for astrocytic glutamate uptake pathway from synaptic cleft. The equations, parameters and variables to create and integrate the new component are presented in this chapter. Also, a qualitative comparison between the new extended synapse model and the original synapse model is presented by graphically showing the dynamical behavior of these models.

4.1 Development of the equations for the astrocytic glutamate uptake

The component of glutamate uptake pathway is composed of four new or modified mathematical equations, describing the glutamate dynamics in different locations during its pathway from the synaptic cleft into the astrocyte, and from the astrocyte into the extrasynaptic space. These equations, in addition to other implementation details required for integrating the glutamate uptake component into the original synapse model, are presented below.

4.1.1 Synaptic glutamate dynamics

In this thesis work, 10 % spillover ($f_{Glu,pre}$) of presynaptically released glutamate from the synaptic cleft back to the presynaptic NMDARs is kept as in the original synapse model presented in [11]. The rest of the glutamate in the synaptic cleft diffuses towards the postsynaptic neuron and astrocyte, both of which can sense the increased glutamate concentration. To be able to describe the faster astrocytic glutamate uptake, compared to the rate of uptake by postsynaptic neuron, the rate constants of glutamate uptake are fitted so that 80-90 % of the glutamate can be seen to go to the astrocyte, and 10-20 % by the postsynaptic neuron.

The dynamics of the synaptic cleft are described in the `postneuron.py` file, so the astrocytic glutamate uptake rate is also described there. Leaning to the finding that EAAT2 is responsible for most of the glutamate uptake [80], only this type of transporter, having a rather high uptake activity, is added to the model in this study. Consequently, the

glutamate uptake ($\frac{\mu M}{ms}$) into astrocyte is described by

$$v_{Glu,uptake,astro} = k_{Glu,uptake,astro}(1 - f_{Glu,pre})[Glu]_{syncleft} \tag{4.1}$$

where $k_{Glu,uptake,astro}$ ($\frac{1}{ms}$) is the rate constant for astrocytic glutamate uptake, thus determining the speed of the uptake. In this approach, $k_{Glu,uptake,astro}$ corresponds to the term g_c and $v_{Glu,uptake,astro}$ to the term $g_c \cdot g$ in Equation (3.6). The way of expressing $v_{Glu,uptake,astro}$ is compliant with the way for modeling the postsynaptic glutamate consumption also in the original synapse model [11].

Glutamate uptake by postsynaptic neuron is described by utilizing the already existing Equation (3.1) for neuronal glutamate consumption from the synaptic cleft. In the equation, the rate constant $k_{Glu,f,post}$ ($\frac{1}{ms}$) determines the speed of neuronal uptake. Neuronal glutamate uptake pathway is not covered in detail in this thesis work, thus there was no need of changing this approach. $k_{Glu,uptake,astro}$ was determined so that $v_{Glu,uptake,astro}$ covers 90 % of the glutamate uptake from the synaptic cleft. The parameter values are listed in Table 4.2 in Section 4.2.

The added astrocytic glutamate uptake now consumes the reservoir of glutamate from the synaptic cleft. To acknowledge this, the Equation (3.4) for glutamate concentration in the synaptic cleft was modified as follows

$$\begin{aligned} \frac{d[Glu]_{syncleft}}{dt} &= -v_{Glu,f,post} - v_{mGluR,f,post} + v_{mGluR,b,post} \\ &-v_{Glu,uptake,astro} + \sum_j \frac{G_{pre} N_{pre} P_{rel,pre} R_{rel,pre}}{k_{Glu,pre} N_A V_{syncleft}} \delta(t - t_j). \end{aligned} \tag{4.2}$$

This change created a need to adapt a few other uptake-related parameters to ensure appropriate fraction of glutamate consumption from the synaptic cleft, as discussed later in Chapter 5.

4.1.2 Astrocytic glutamate dynamics

In the astrocyte model file of the new model, the intracellular glutamate concentration is initialized to zero. As explained earlier, some of the uptaken glutamate is converted into glutamine. However, for simplicity, glutamate and glutamine are treated here as the same molecule. This intracellular glutamate concentration then changes with respect to glutamate uptake from the synaptic cleft and extrasynaptic space, and the amount of glutamate that is released into extrasynaptic space. The intracellular astrocytic glutamate dynamics is described as

$$\frac{d[Glu]_{astro}}{dt} = \frac{1}{r_{vesext,astro}} r_{astro}[Glu]_{extsyn} + r_{cleft,astro} v_{Glu,uptake,astro} - \sum (Glu_{astro} P_{rel,astro} R_{rel,astro}) \delta(t - \tau_i). \tag{4.3}$$

The term $\frac{1}{r_{vesext,astro}} r_{astro}[Glu]_{extsyn}$ describes the glutamate uptake from extrasynaptic space. It corresponds to the term $Glu_{E \to A}(t)$ in Equation (3.7). The term r_{astro} is the clearance rate of glutamate from the extrasynaptic space, and $[Glu]_{extsyn}$ is the glutamate concentration in the extrasynaptic space. The variable $r_{cleft,astro}$ is the ratio between volume of the synaptic cleft and volume of the astrocyte, which scales the concentration value to the correct volume. The summation term describes the amount of glutamate that is released from the astrocyte, and it corresponds to the term V_{gme} in Equation (3.7).

The original model presented the glutamate dynamics in the extrasynaptic space between the astrocyte and the presynaptic neuron, according to the Equation (3.5). The glutamate concentration in the extrasynaptic space depends on the concentration of astrocytic glutamate. Thus, the released glutamate is now mediated by the new variable $[Glu]_{astro}$ instead of G_{astro} (Equation (3.5)). In addition, G_{astro} described one astrocytic vesicle pool, which was in the original synapse model multiplied with number of releasable vesicle pools, N_{astro}. In the new synapse model, $[Glu]_{astro}$ describes the glutamate concentration in the whole astrocyte, covering the whole term $G_{astro} \cdot N_{astro}$. Thus, in the new implementation, the extrasynaptic glutamate dynamics is presented as

$$\frac{d[Glu]_{extsyn}}{dt} = -r_{astro}[Glu]_{extsyn} + \sum_i r_{vesext,astro}[Glu]_{astro} P_{rel,astro} R_{rel,astro} \delta(t - \tau_i). \tag{4.4}$$

All modified and developed mathematical expressions are expressed as code in Table 4.1. The Table 4.1 includes also all other modifications to the original code that are crucial for the reproduction of the new synapse model implementation.

Table 4.1. *The implementation of the astrocytic glutamate uptake pathway required modifications in some of the existing equations, as well as a few completely new equations and commands. The code file locations of the expressions are also presented.*

File and line	Code	Description
astrocyte.py, line 91	`def derivative(self, AG_post, r_leakER_astro, v_Glu_Uptake_Astro)`	`v_Glu_Uptake_Astro` added to the function parameters
astrocyte.py, line 127	`"Glu_astro": 1/p["r_vesext_astro] * p["r_astro"] * x["Glu_extsyn"] + v_Glu_Uptake_Astro`	Adding the uptaken glutamate into the initial astrocytic glutamate value
astrocyte.py, line 219	`x["Glu_astro"] -= x["Glu_astro"] * p["Prel_astro"] * Rrel_astro_old`	Updating the delta term for the astrocytic glutamate value
postneuron.py, line 409	`v_Glu_Uptake_Astro = p["k_Glu_Uptake_Astro"] * (1 - f_Glu_pre) * x["Glu_syncleft"]`	Astrocytic glutamate uptake rate
postneuron.py, line 566	`"Glu_syncleft": -v_Glu_f_post -v_mGluR_f_post - v_Glu_Uptake_Astro + v_mGluR_b_post`	Updating the glutamate concentration in synaptic cleft (delta term was not modified)
postneuron.py, line 579	`"v_Glu_Uptake_Astro": v_Glu_Uptake_Astro`	Return the uptake parameter
run_pairings.py, line 45	`"Glu_astro": astro["Glu_astro"]`	Returning the state variable of astrocytic glutamate concentration
run_pairings.py, line 197	`deriv_astro, other_var_ast = astro.derivative(post.x["AG_post"], ..., other_var_post["v_Glu_Uptake_Astro"]`	Saving the glutamate uptake rate to the astrocytic variables for plotting purposes
run_pairings.py, line 249	`other_var = "f_pre": f_pre, ..., "v_Glu_Uptake_Astro": other_var_post["v_Glu_Uptake_Astro"]`	Saving the astrocytic glutamate uptake variable for plotting purposes before and after t-LTD induction
run_before_and_after_pairings.py, line 44	`"Glu_astro": astro["Glu_astro"]`	Returning the state variable of astrocytic glutamate concentration
run_before_and_after_pairings.py, line 189	`deriv_ast, other_var_ast = astro.derivative(post.x["AG_post"], ..., other_var_post["v_Glu_uptake_astro"]`	Saving the glutamate uptake rate to the astrocytic variables for plotting purposes during t-LTD induction

4.2 Glutamate uptake parameters

To incorporate the new glutamate uptake function to the original implementation of the synapse model, some parameters needed to be modified but also some new parameters and initial values were to be added. These parameters and initial values are presented and used in the Equations (4.1)–(4.4), and summarized in Table 4.2.

Table 4.2. *Modified and added parameters and initial values required for the new implementation. Their locations in the code files are also presented. The values are either based on previous experimental data or the behavior of the original synapse model.*

File and line	Parameter	Value	Description
postneuron.py line 167	$k_{Glu,uptake,astro}$	0.18 $\frac{1}{ms}$	Rate constant for astrocytic glutamate uptake by glutamate transporter. Based on transporter dynamics between neurons and astrocyte, and the model behavior.
postneuron.py line 166	$k_{f,glu,post}$	0.02 $\frac{1}{ms}$	Rate constant for neuronal glutamate consumption. Modified from [11] and [98].
postneuron.py line 206	$v_{Glu,uptake,astro}$	0 $\frac{\mu M}{ms}$	Initial value for astrocytic glutamate uptake
astrocyte.py line 18	$[Glu]_{astro}$	0 μM	Initial value for astrocytic glutamate concentration
astrocyte.py line 47	$r_{cleft,astro}$	15	Ratio between volume of the synaptic cleft and volume of the astrocyte, developed to scale the uptake rate of astrocytic glutamate based on the model behavior.

Some of these parameter values are based on, or adapted from, theoretical or experimental data. However, due to the lack of experimental data for astrocytic glutamate transporters, some values were based on the original model behavior.

4.3 Evaluation of the new synapse model

The new synapse model was closely optimized to reproduce the dynamics of the original synapse model implemented by Manninen et al. [11]. After integrating the completely new astrocytic glutamate uptake component to the original model, it was not possible to completely mimic the initial model dynamics. Some compromises were done to fit the output of the new implementation to a level that was considered to be accurate enough for this thesis work.

The variation of the two new variables, astrocytic glutamate uptake (Equation (4.1)) and concentration for intracellular astrocytic glutamate (Equation (4.3)), at temporal difference of ΔT = −10ms during t-LTD induction, are presented in Figure 4.1. The performance between the original and the new synapse model can be compared by viewing the Figures 4.2, 4.3, 4.4 and 4.5.

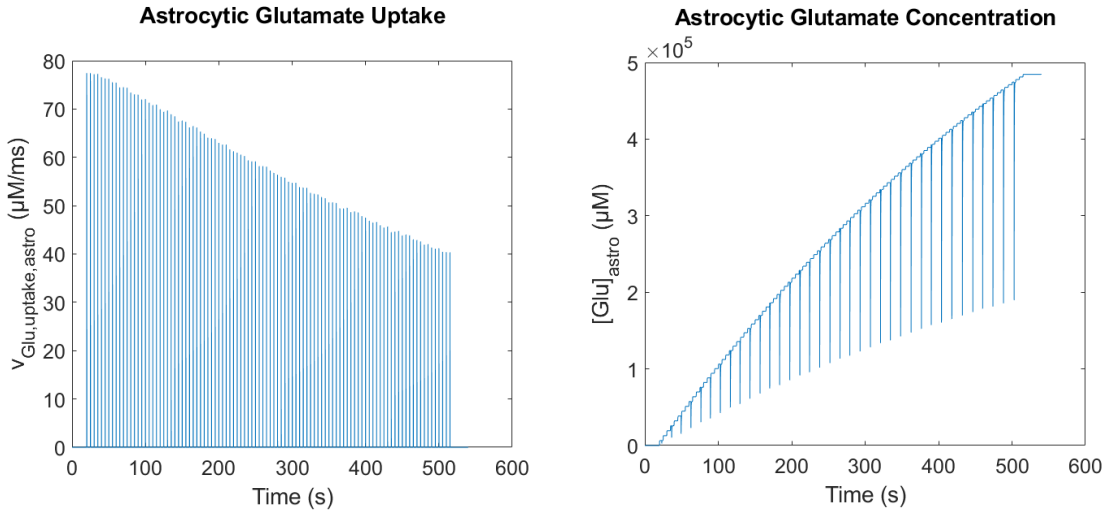

Figure 4.1. *Astrocytic glutamate uptake and intracellular glutamate concentration during t-LTD induction at temporal difference of $\Delta T = -10$ ms. This data is used as a baseline for astrocytic glutamate uptake and concentration in this thesis work.*

The glutamate concentration and uptake rate in Figure 4.1 present the level of astrocytic glutamate dynamics that are considered as normal for this work. These values may not yet be biological, and they would require more validation against experimental data. However, the results in Figure 4.1 can be used as a baseline for evaluating the function of this model. The peak value for astrocytic glutamate uptake rate in the normal dynamics of this model reaches almost 80 $\frac{\mu M}{ms}$, and decreases with time, responding to the t-LTD induction. The t-LTD induction decreases the strength and efficiency of the synapse, causing the postsynaptic potential to decrease. This leads also to smaller release probability of the presynaptic glutamate, which explains the descending uptake activity. The presynaptic glutamate release probability has been shown to decrease during t-LTD induction [7], leading to less glutamate in the synaptic cleft, and thus lower activity required for glutamate uptake. Astrocytic glutamate concentration in Figure 4.1 seems to increase even though the uptake activity decreases, despite that the pulses of glutamate release increase relatively.

Figures 4.2 and 4.3 show the responses of the pre- and postsynaptic neurons to the t-LTD stimulation protocol, performed with the original synapse model and the new implementation, respectively. The explanation of the stimulation protocol can be reviewed from Section 3.1.1 and Figure 3.2. The results in Figures 4.2 and 4.3 present six key model variables during the three different phases of the stimulation protocol: (1) Subfigures B–G

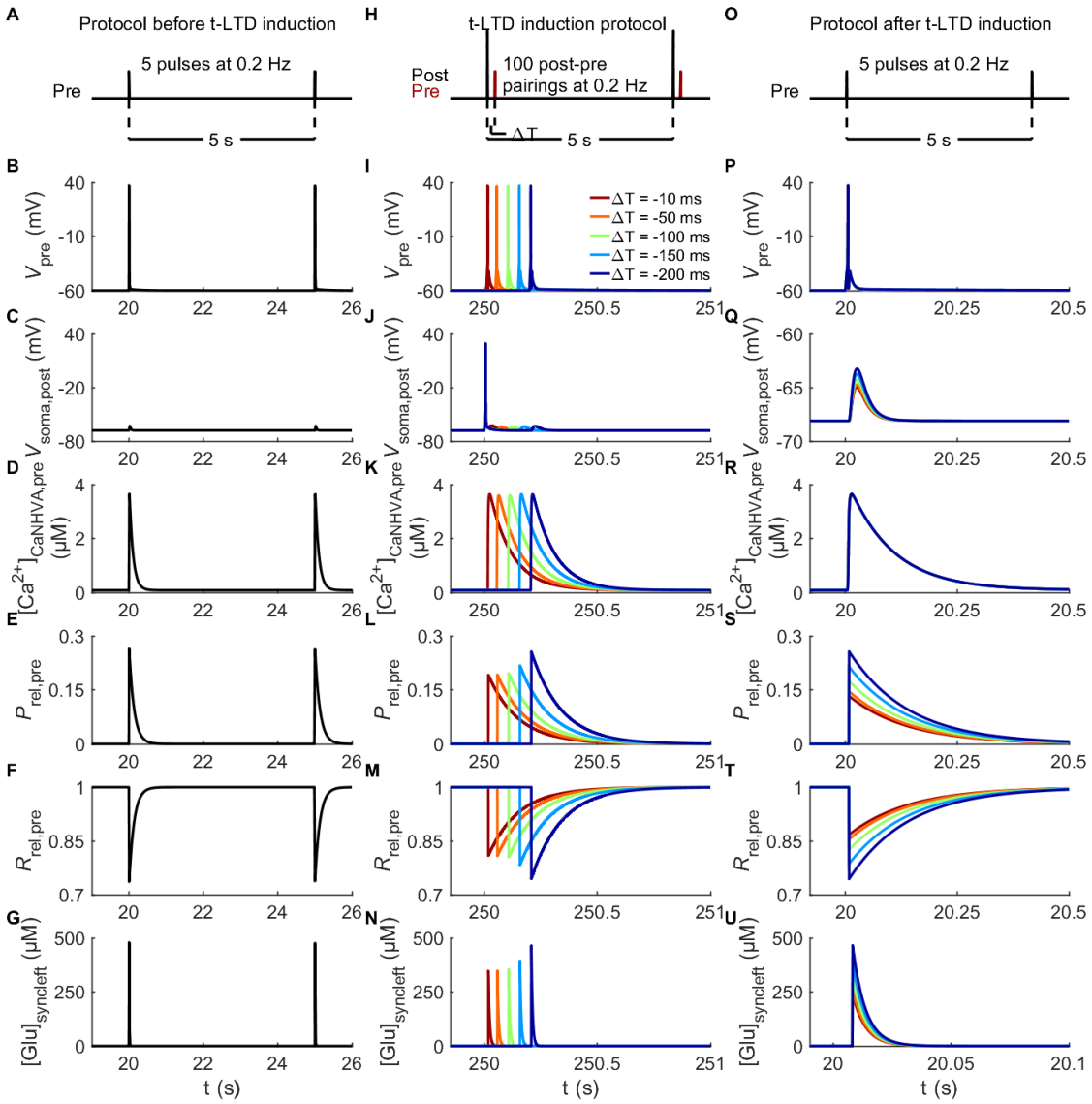

Figure 4.2. *Responses of the pre- and postsynaptic neurons in the original synapse model to the t-LTD stimulation protocol. The stimulation protocol is presented in Figure 3.2. The simulation results present five key pre- and postsynaptic variables and one variable describing the glutamate concentration in the synaptic cleft. Subfigures B-G on the left column present the responses before t-LTD induction during the first two pulses of the protocol before t-LTD induction; I-N present the responses with five different temporal differences during one post-pre pairing of the t-LTD induction; and P-U present the responses after t-LTD induction. Note the different scale of the x-axis in U, compared to the ones in P–T.*

in the left column present the responses during the first two stimulus pulses of the stimulation protocol before t-LTD induction; (2) Subfigures I–N in the middle column present the responses during one post-pre pairing, with the chosen five different ΔT values (Section 3.1.1), at approximately halfway of the 100 post-pre pairings of the t-LTD induction; (3) Subfigures P–U in the right column present the responses after t-LTD induction, for a single stimulus pulse. Note the different scale of the x-axis in U compared to P–T.

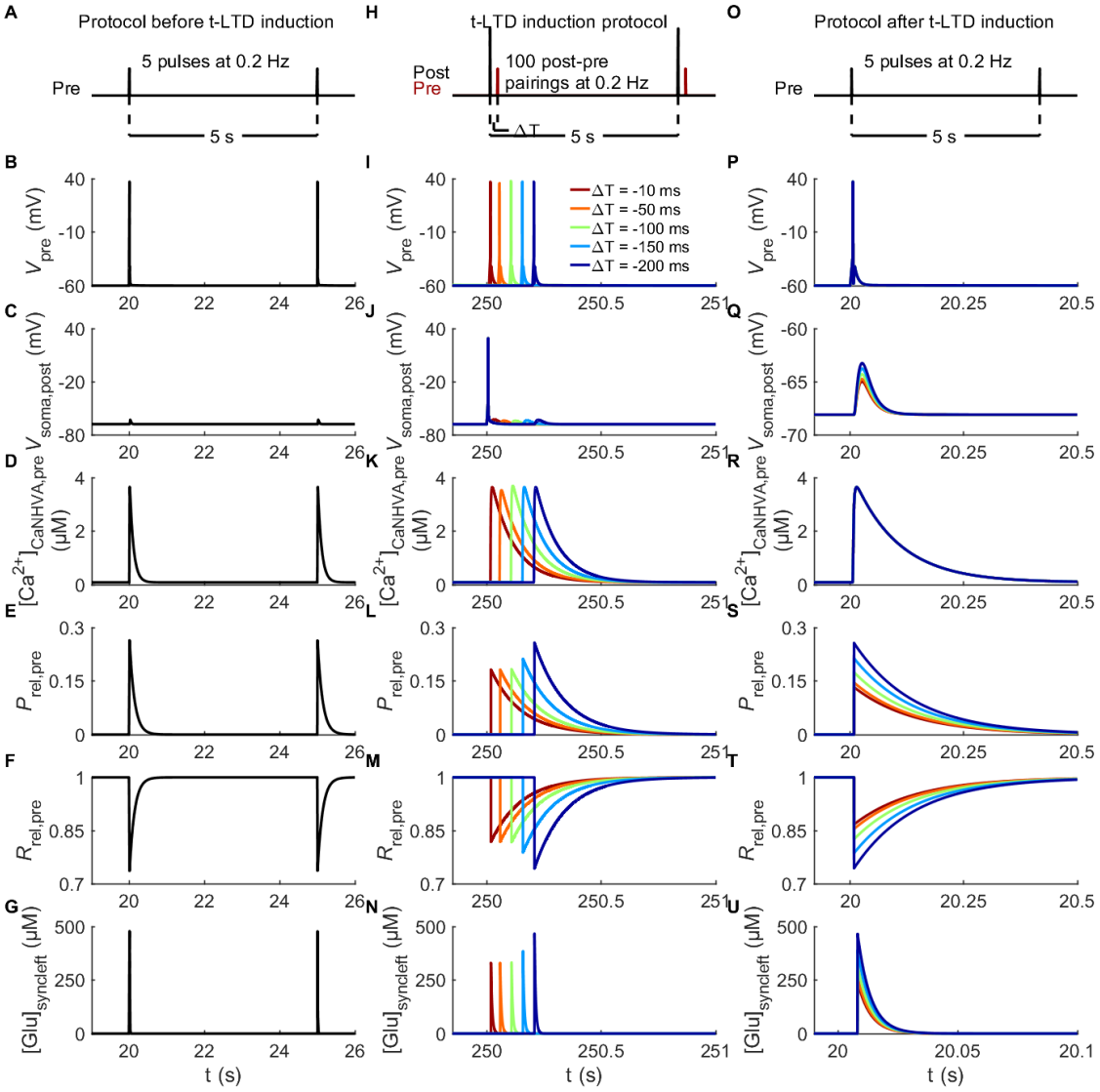

Figure 4.3. *Responses of the pre- and postsynaptic neurons to the t-LTD stimulation protocol in the new synapse model. When compared to the original responses presented in Figure 4.2, the results can be perceived to be rather identical.*

In Figures 4.2 and 4.3, V_{pre} presents the presynaptic membrane potential, $V_{soma,post}$ is the postsynaptic membrane potential, $[Ca^{2+}]_{CaNHVA,pre}$ is the presynaptic Ca^{2+} concentration mediated by Ca_{NHVA} channels, $P_{rel,pre}$ is the release probability of presynaptic glutamate vesicles, $R_{rel,pre}$ is the fraction of releasable presynaptic vesicles, and $[Glu]_{syncleft}$ is the glutamate concentration in the synaptic cleft. Some of the variables presented here, for example $[Ca^{2+}]_{CaNHVA,pre}$ (for more details, see [11]), are included in this presentation for the purpose of comparison, and it is not of importance to understand variables that have not been introduced in the theoretical part of this work. In the evaluation of the new synapse model, it is important to compare all key variables that were originally used to describe the dynamics of the original model. This helps to ensure that the new model behaves similarly compared to the original model in terms of the most important presynaptic, postsynaptic and astrocytic variables.

Regarding the results presented in Figure 4.3, the new implementation performs almost identically compared to the original synapse model. For example, in both implementations, the t-LTD induction with $\Delta T = -10ms$ results in the lowest release probability of presynaptic glutamate (Figures 4.3L and S), and thus the lowest synaptic glutamate concentration (Figures 4.3N and U). The most critical variable to compare from this first set of results is the glutamate concentration in the synaptic cleft, due to the addition of a new component of consuming glutamate outwards the cleft.

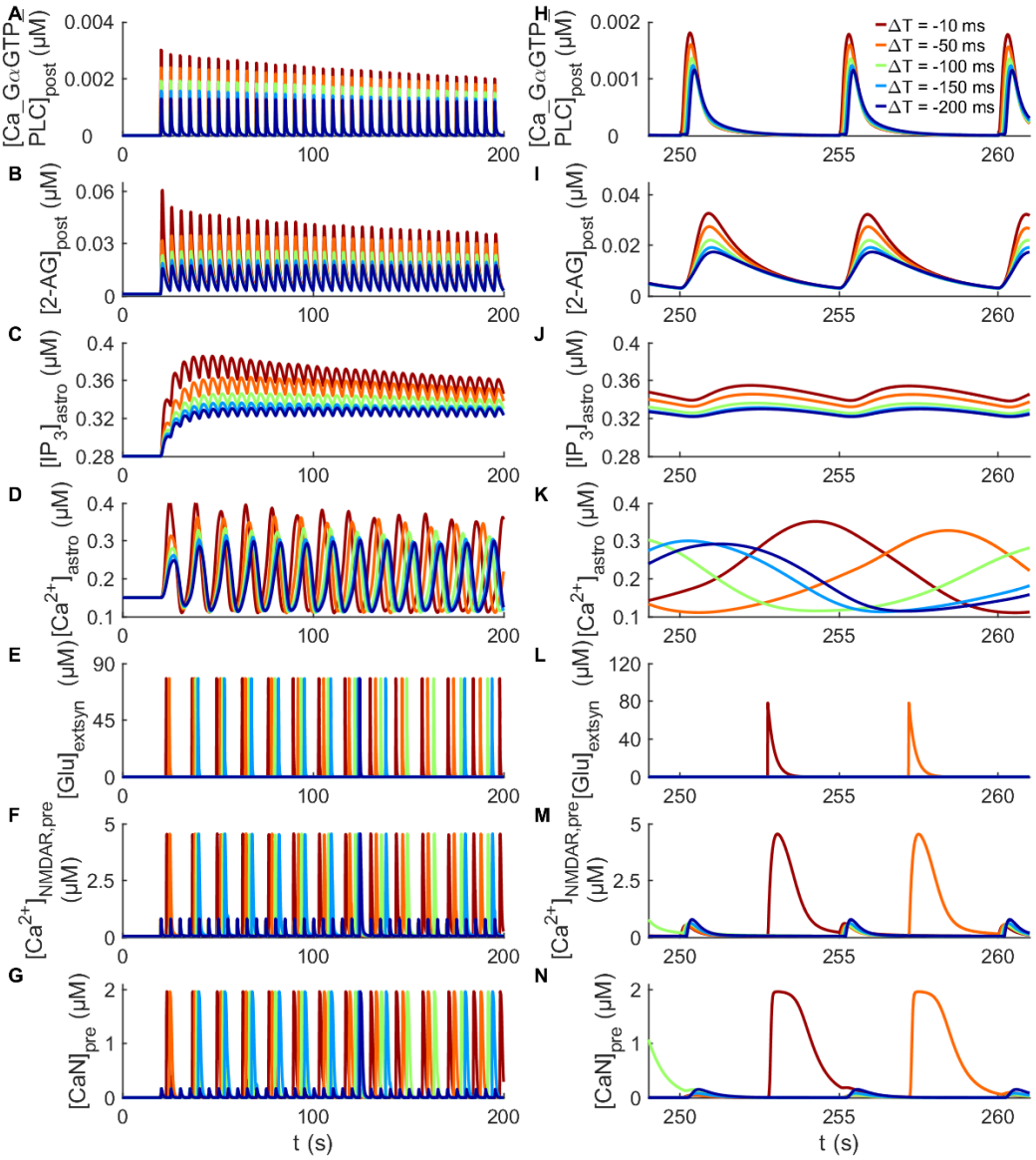

Figure 4.4. *Postsynaptically released endocannabinoid 2-AG activates astrocytic Ca^{2+} signaling, which is followed by astrocytic glutamate release. Astrocytically released glutamate activates presynaptic (NMDARs) which leads to activation of presynaptic Ca^{2+} and CaN. These results are obtained with the original implementation of the synapse model, during the t-LTD induction stimulation protocol with five different temporal differences. The right column (A-G) presents the modeled variables during the first 200s of the t-LTD induction. The left column (H-N) presents the same variables in a narrower time window occurring approximately in the middle of the protocol.*

Figures 4.4 and 4.5 show the presynaptic, postsynaptic and astrocytic variables important for the signaling cascade originating from the postsynaptic endocannabinoid production, all the way to the release of glutamate from the astrocyte to the extrasynaptic space during the t-LTD induction. Figure 4.4 is the output of the original synapse model, and Figure 4.5 is the output of the new model. All variables presented in Figures 4.4 and 4.5 are affected by the modified expressions in the new synapse model. Thus, this set of neuronal and astrocytic responses is the most sensitive to any deviations of the model dynamics.

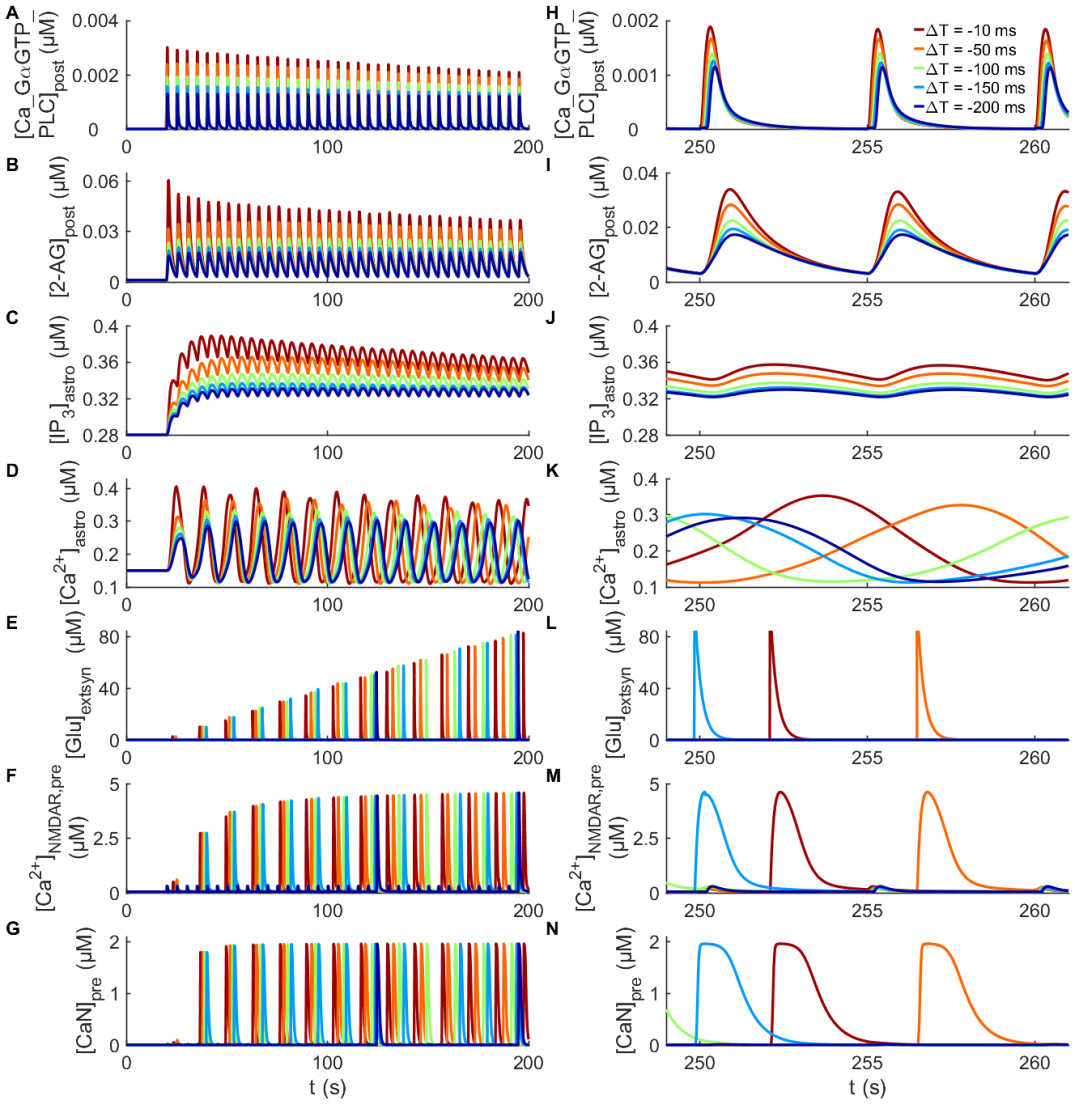

Figure 4.5. *The new synapse model performed in a slightly different way compared to the corresponding results in Figure 4.4, obtained with the original model. The difference in the dynamical behaviour can be seen from Subfigures E, F, G, L, M and N. The pulse-like increases in the glutamate concentrations of the extrasynaptic space increases with time, which also affects the presynaptic Ca^{2+} and CaN concentrations. An additional increase in extrasynaptic glutamate concentration occurs at 250s for temporal difference of -150ms, causing corresponding increases in the concentrations of presynaptic Ca^{2+} and CaN. Note the different y-axes of Subfigures E and L between Figures 4.4 and 4.5.*

In Figures 4.4 and 4.5, Ca^{2+}-GαGTP-PLC describes a complex that is formed following the activation of the postsynaptic mGluR-mediated signaling cascade. This signaling cascade leads to the formation of postsynaptic 2-AG. $[IP_3]_{astro}$ is the astrocytic IP_3 concentration, $[Ca^{2+}]_{NMDAR,pre}$ describes the Ca^{2+} concentration mediated by activation of presynaptic NMDARs, and $[CaN]_{pre}$ is the presynaptic CaN concentration. The concentration of CaN depends on the presynaptic Ca^{2+}, and it affects the next cycle of vesicular glutamate release from the presynaptic neuron.

Thus, Figures 4.4 and 4.5 describe the dynamics where postsynaptically released endocannabinoid 2-AG activates astrocytic Ca^{2+} signaling, followed by astrocytic glutamate release. The Ca^{2+} signaling has slower dynamics than the release of glutamate, which can be seen especially from subfigures K and L in Figures 4.4 and 4.5. The astrocytically released glutamate activates presynaptic NMDARs, which leads to an increase in the concentrations of presynaptic Ca^{2+} and CaN. The results are obtained during the t-LTD induction stimulation protocol with five different temporal differences. The left column (A-G) presents the modeled variables during the first 200s of the t-LTD induction. The right column (H-N) presents the same variables in a narrower time window occurring approximately in the middle of the t-LTD induction protocol.

In practise, Figures 4.4 and 4.5 demonstrate the increase of astrocytic Ca^{2+} signaling due to postsynaptic 2-AG release. When the astrocytic Ca^{2+} exceeds the threshold value of 0.3 μM, a pulse-like glutamate release from astrocyte is induced, leading to an increase in the extrasynaptic glutamate concentration. These results show some variations between the function of the original and the new model, mainly as a more dynamical nature of the response and a higher maximum value of the extrasynaptic glutamate concentration in the new model. This affects slightly also the responses of presynaptic Ca^{2+} and CaN concentrations. Also, an additional increase in the extrasynaptic glutamate occurs at ΔT = $-$150ms, leading to corresponding increases in the activation of presynaptic NMDARs and thus in the concentrations of presynaptic Ca^{2+} and CaN.

The signaling cycle of this neuron-astrocyte interaction, supporting the understanding of the relation of these variables presented in Figures 4.2–4.5, can be reviewed from the synapse model illustration from Figure 3.1. The two synapse models behave identically enough for the new model to be further tested. However, the results presented in the Sections 4.1–4.3 are considered the main results of this work.

4.4 Relationship between astrocytic glutamate uptake and the new model dynamics

To study in more detail the function of the new implementation, the relationship of astrocytic glutamate uptake to the new model dynamics is briefly examined. At the same time,

the results are used to obtain preliminary computational data on how the stimulation of the t-LTD induction protocol reacted to the modifications of the glutamate uptake.

The further testing is performed with three different conditions: (1) astrocytic glutamate uptake rate is increased while neuronal uptake rate remained the same (Figures 4.6 and 4.7), (2) astrocytic glutamate uptake rate is decreased, similarly keeping the neuronal uptake rate as the same (Figures 4.8 and 4.9), and (3) astrocytic glutamate uptake is completely blocked (Figures 4.10 and 4.11). The same set of model variables used in Figures 4.4 and 4.5 are used to present the results also in Figures 4.7, 4.9 and 4.11. Note the different y-axes between the figures.

The values for the increased astrocytic glutamate uptake rate and intracellular astrocytic glutamate concentration are presented in Figure 4.6. The applied reaction rate constant for astrocytic glutamate uptake is set as $k_{Glu,Uptake,Astro}$ = 0.3 $\frac{1}{ms}$, with what the uptake rate reaches a maximum of approximately 130 $\frac{\mu M}{ms}$. The increased value for the reaction rate constant for astrocytic glutamate uptake is an estimate for evaluation purposes and is not based on previous experimental studies.

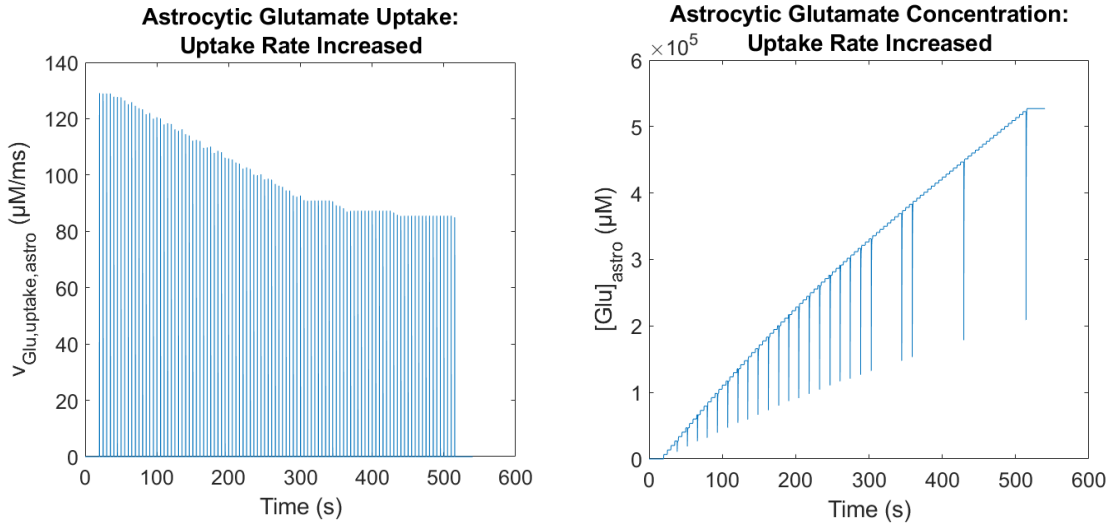

Figure 4.6. *Increased astrocytic glutamate uptake and intracellular glutamate concentration during t-LTD induction at temporal difference of $\Delta T = -10$ ms.*

Results in Figure 4.7 show that, as expected, the increased astrocytic glutamate uptake leads to glutamate being consumed too fast from the synaptic cleft. This leads to a situation where there is not enough glutamate in the synaptic cleft to activate the postsynaptic receptors as required. This causes lower magnitude of the intracellular postsynaptic signaling cascade leading to production of 2-AG, and eventually leads to a decreased astrocytic Ca^{2+} signaling. The concentration of astrocytic Ca^{2+} rarely reaches the threshold value of 0.3 μM at longer temporal differences, leading to less frequent release of glutamate from the astrocyte at ΔT = $-$150 ms (Figure 4.7L). This is shown in less frequent

activation of presynaptic NMDARs, and thus less frequent increases in the presynaptic Ca^{2+} (Figure 4.7M), and presynaptic CaN concentrations (Figure 4.7N) at $\Delta T = -150$ ms. The timing of signaling at other temporal differences is also affected.

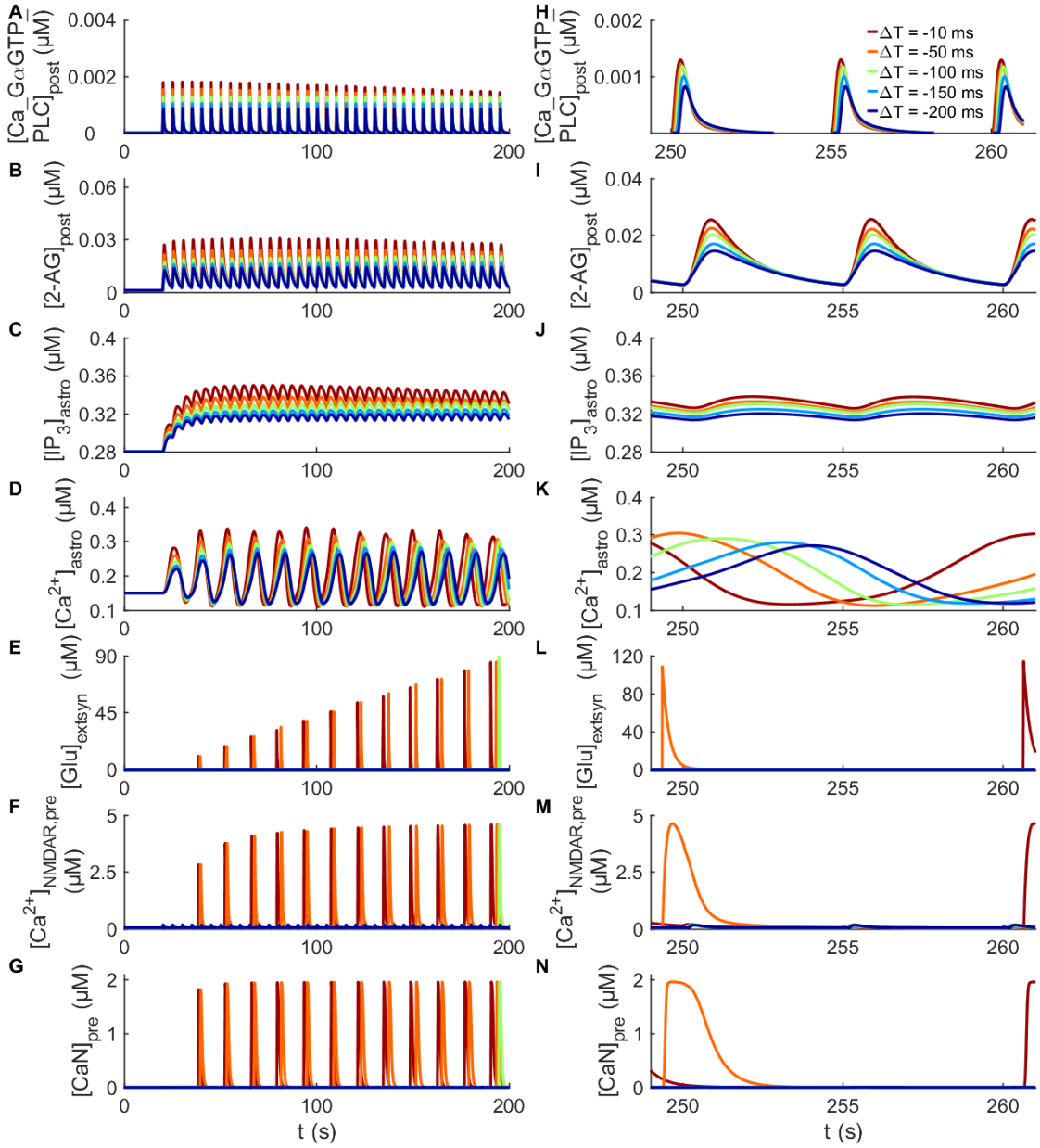

Figure 4.7. *Responses of six key presynaptic, postsynaptic and astrocytic variables during the t-LTD induction in the new synapse model, when astrocytic glutamate uptake is increased. Note the different y-axis in L compared to Figure 4.5.*

Figures 4.8 and 4.9 present the condition of decreased astrocytic glutamate uptake. The rate of astrocytic glutamate uptake and intracellular astrocytic glutamate concentration are presented in Figure 4.8. The decreased uptake rate reaches approximately 43 $\frac{\mu M}{ms}$ at maximum. To describe a decrease in astrocytic glutamate uptake rate, value of $k_{Glu,Uptake,Astro}$ = 0.1 $\frac{1}{ms}$ is used. This value is also not based on experimental data.

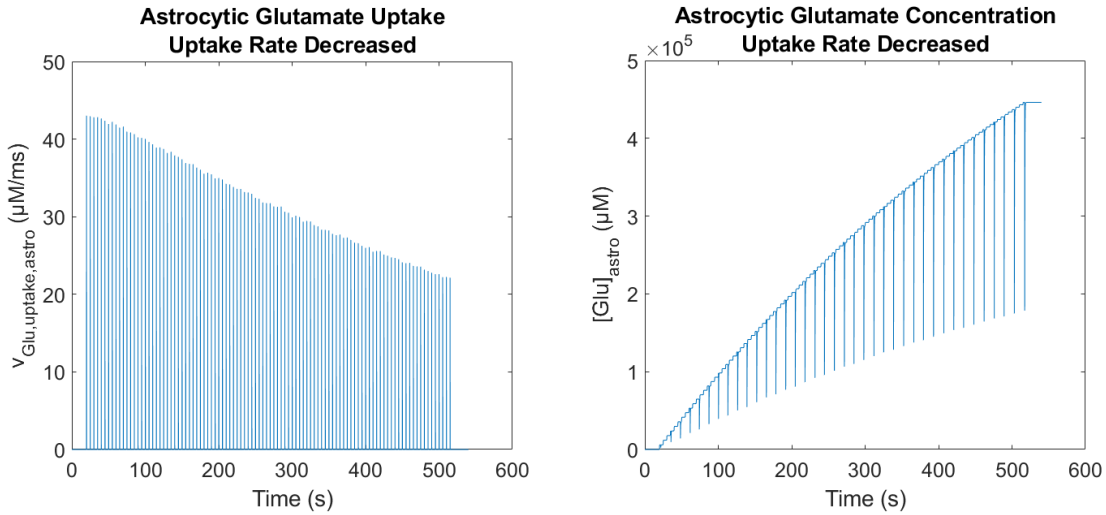

Figure 4.8. *Decreased astrocytic glutamate uptake and intracellular glutamate concentration during t-LTD induction at temporal difference of $\Delta T = -10$ ms.*

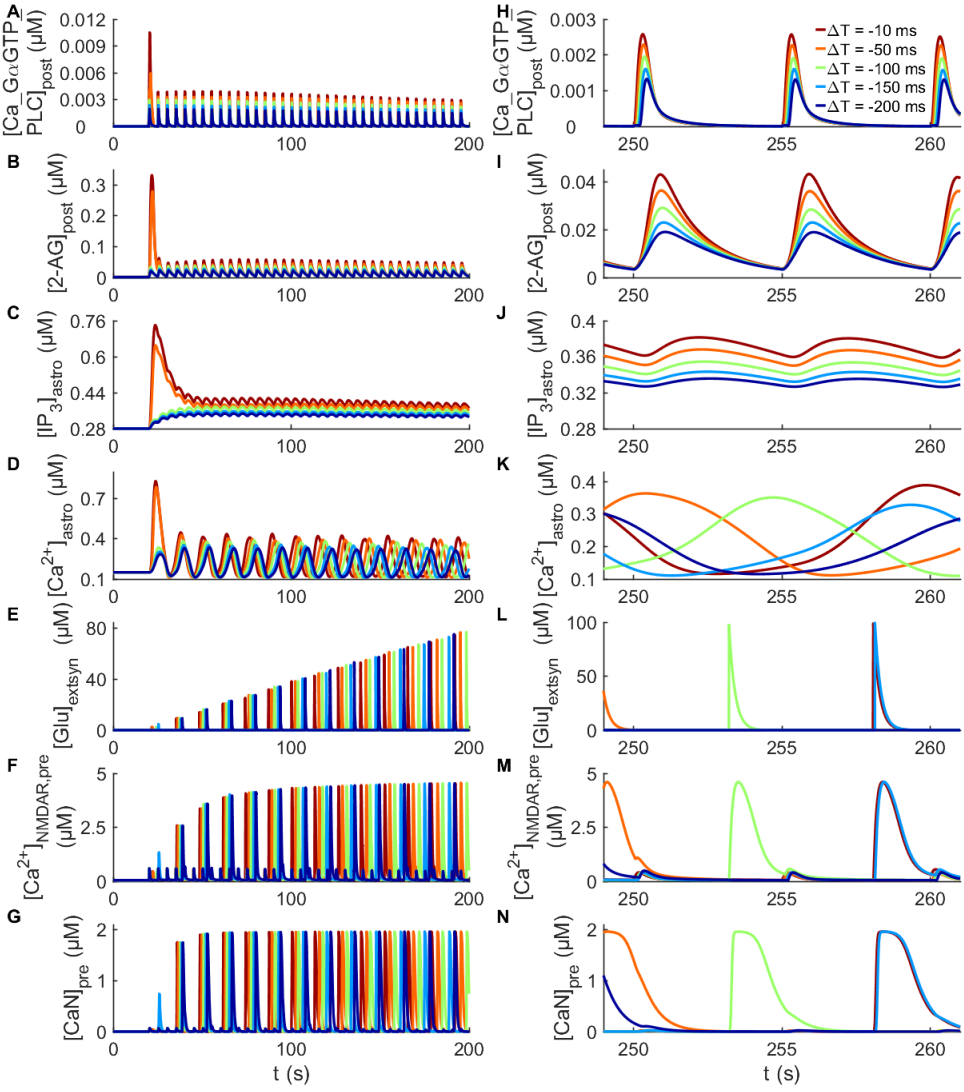

Figure 4.9. *Responses of six key presynaptic, postsynaptic and astrocytic variables during t-LTD induction in the new synapse model, when astrocytic glutamate uptake is decreased. Note the different y-axes in A–E and H compared to the Figure 4.5.*

Results in Figure 4.9 show the opposite situation compared to Figure 4.7. The astrocytic glutamate uptake rate is decreased, leading to excess activation of postsynaptic receptors. As presumed, the concentration of intracellular postsynaptic 2-AG is increased, eventually leading to an increase in astrocytic Ca^{2+} signaling with all temporal differences. Furthermore, this leads to more frequent increases in the extrasynaptic glutamate (Figure 4.9L). Higher extrasynaptic concentration leads to higher activation of presynaptic NMDARs and thus higher concentrations of presynaptic Ca^{2+} (Figure 4.9M) and CaN (Figure 4.9N) at ΔT = $-$100ms and ΔT = $-$150ms. The signaling during other temporal differences is also affected. Note the different y-axes compared to the Figure 4.5, especially for the responses of postsynaptic 2-AG, astrocytic IP_3 and astrocytic Ca^{2+} in Figures 4.9A, B and C, respectively.

Lastly, Figures 4.10 and 4.11 present the condition where astrocytic glutamate uptake is completely blocked. This is described by setting the $k_{Glu,Uptake,Astro}$ as 0 $\frac{1}{ms}$. The corresponding astrocytic glutamate uptake rate and intracellular astrocytic glutamate concentration are shown in Figure 4.10. The small increase in the intracellular glutamate, seen from Figure 4.10, is due to the uptake from the extrasynaptic space, described with the term $\frac{1}{r_{vesext,astro}} r_{astro}[Glu]_{extsyn}$ in Equation (4.3).

When astrocytic glutamate uptake is completely blocked, it leaves the postsynaptic neuron responsible for all the glutamate clearance, even though the neuronal glutamate consumption is not increased.

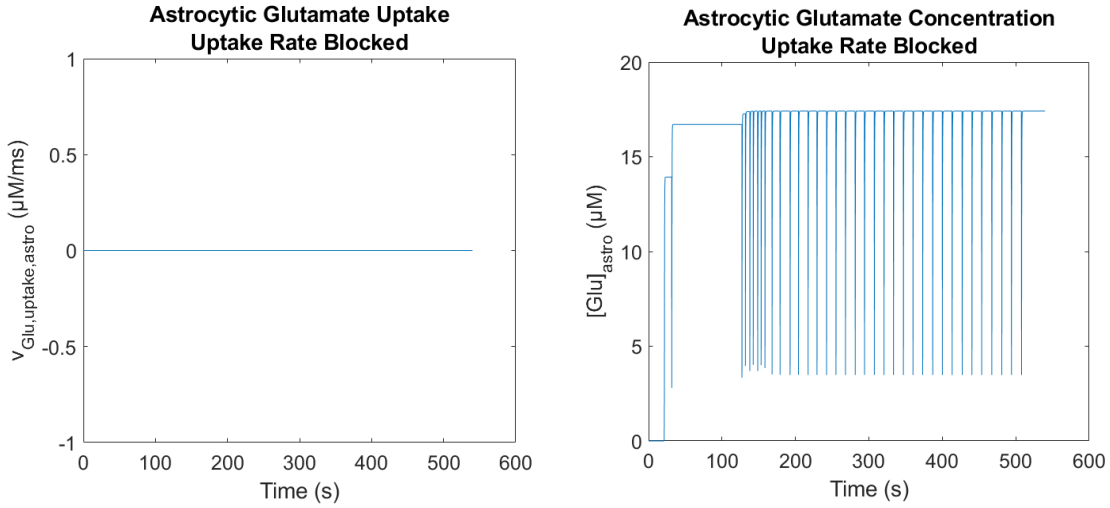

Figure 4.10. *Astrocytic glutamate uptake and intracellular concentration when the uptake rate was blocked. The small increase in the intracellular glutamate concentration is due to uptake from extrasynaptic space.*

This has, as expected, similar but magnified effect on the responses of the model variables than in the previous condition where the uptake rate was decreased. Thus, the

postsynaptic reactions in Figure 4.11A–C and H–J follow similar trends as in Figure 4.9, however with larger magnitude.

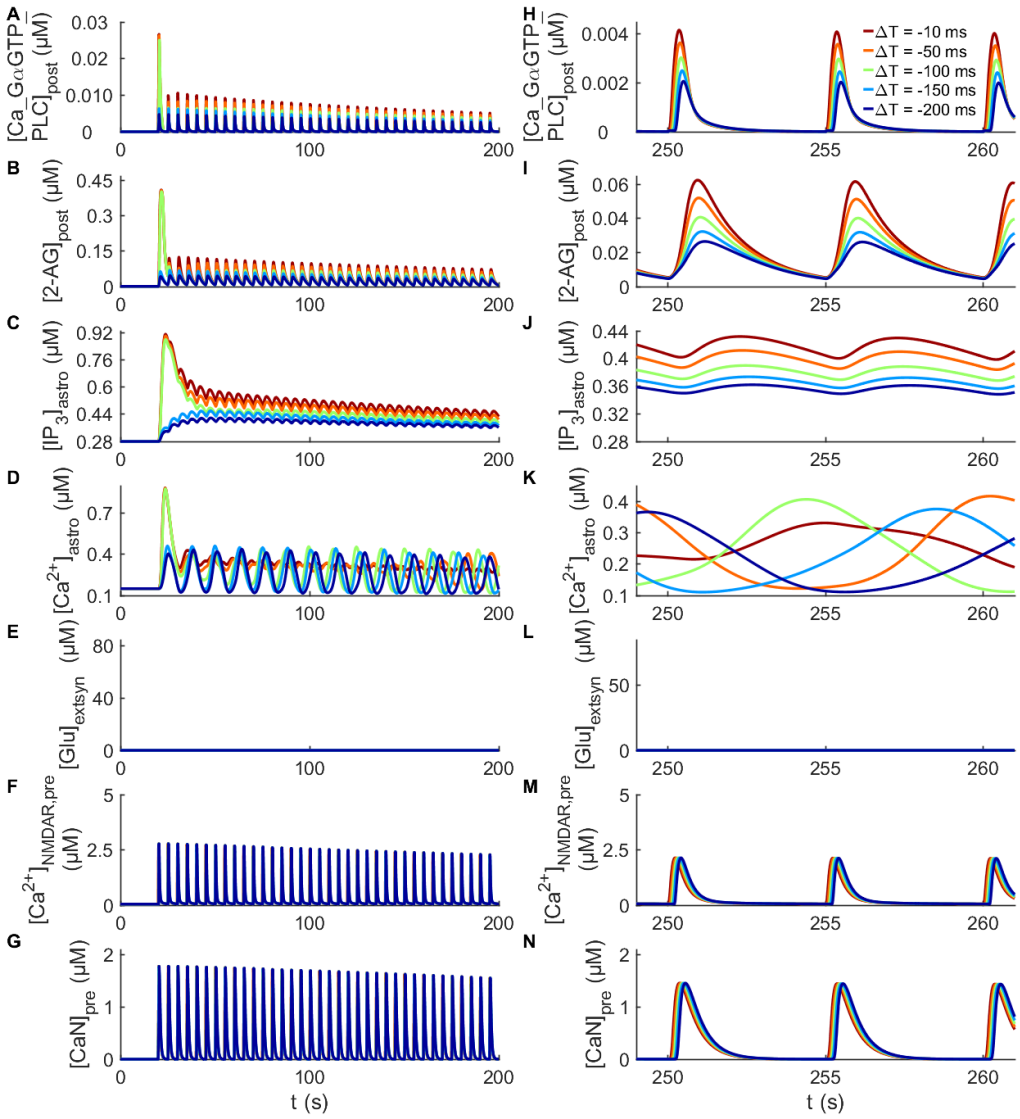

Figure 4.11. *Responses of six key presynaptic, postsynaptic and astrocyte related variables during t-LTD induction in the new synapse model, when astrocytic glutamate uptake is blocked. Note the different y-axes in A–D and H–I compared to the Figure 4.5.*

When astrocytic glutamate is blocked, there is not enough glutamate to be released. Thus, the extrasynaptic glutamate concentration stays close to 0, leading to significantly decreased concentration of presynaptic Ca^{2+} and CaN at all temporal differences (Figures 4.11E–F and L–N). Note the different y-axes in A–D and H–I compared to the results in Figure 4.5. When the glutamate uptake was blocked, the increases in the first pulses of postsynaptic 2-AG, astrocytic IP_3 and astrocytic Ca^{2+} concentrations were even more notable.

5. DISCUSSION

In this thesis work, a novel implementation of astrocytic glutamate uptake pathway from synaptic cleft was developed into a previously published synapse model by Manninen et al. [11]. The developed component connects the pathway for glutamate from presynaptic neuron to the synaptic cleft, from the synaptic cleft to the astrocyte, and finally from the astrocyte to the extrasynaptic space where it activates the glutamate receptors on the presynaptic neuron.

A few assumptions and simplifications were made to accomplish the functionality of the developed implementation of the astrocytic glutamate uptake from synaptic cleft. All the glutamate taken up by the astrocyte was assumed to be available for recycling in the so-called glutamate-glutamine cycle. In other words, all the intracellular astrocytic glutamate was taken into account when determining the amount of glutamate released from the astrocyte. In reality, there are also other ways to recycle or re-use glutamate: some of the astrocytic glutamate is metabolized and used in other intracellular processes in the astrocyte [59]. Also, before being released from the astrocyte, glutamate can be converted into glutamine. In the model, glutamate and glutamine were treated as the same molecule and this conversion was ignored. This did not, however, have any significant effect on the model, and is a commonly utilized simplification also in previously published models [99].

The astrocytic glutamate uptake, $v_{Glu,uptake,astro}$, presented in Equation (4.1) was created to demonstrate the glutamate uptake by astrocytic glutamate transporter. The transporter dynamics, in this case the uptake rate, was adapted from the properties of EAAT2. The similarity of the expressions for $v_{Glu,uptake,astro}$ and postsynaptic glutamate consumption $v_{Glu,f,post}$ (presented in Equation (3.1)) made it possible to control their relative ratio rather easily. This was done by fitting the rate constants, $k_{Glu,uptake,astro}$ and $k_{f,Glu,post}$, to represent the share of the astrocytic glutamate uptake as 90 % and the neuronal glutamate uptake as 10 %.

Also other aspects of the model implementation were to be considered when fitting the ratio of the reaction rate constants. The glutamate dynamics in the synaptic cleft are dependent partly on the glutamate uptake, according to the Equation (4.2). Thus, the rate constants were not only fitted with respect to each other, but also against the synaptic glutamate concentration. Experimental data shows that the glutamate in the synaptic

cleft can reach 1 mM following the presynaptic release [71]. In the synapse model, the maximum concentration of glutamate in the synaptic cleft reached 500 µM at best, which allows the concentration of presynaptically released glutamate to be doubled. However, due to numerical limitations restricting the glutamate concentration in the synaptic cleft, the maximum value of presynaptically released glutamate could not be increased without overflow error in Python. The possibility of increasing the maximum value could be addressed in the future, if needed, but it would require more extensive optimization between the new and original expressions of the dynamics in the synaptic cleft.

This current restriction of the glutamate concentration in the synaptic cleft strongly determined the maximum values for astrocytic and neuronal uptakes because the activation of postsynaptic receptors, and thus postsynaptic intracellular signaling cascades, are dependent on the glutamate concentration in the synaptic cleft. In the original synapse model, the value of $k_{f,Glu,post}$ was 10 times higher (0.2 $\frac{1}{ms}$) compared to the value chosen for the implementation of the new synapse model (0.02 $\frac{1}{ms}$). In practice, this meant that the neuronal consumption was originally 20 % of the synaptic glutamate, and 80 % was available to be used to activate the receptors. To preserve the correct activation rate of postsynaptic receptors, the astrocyte and neuronal glutamate uptakes were allowed to consume this 20 % in total. To follow the correct ratio between these two glutamate pathways and still reach realistic signaling cascades with the model, the optimized rate constants were set as 0.18 $\frac{1}{ms}$ for $k_{Glu,uptake,astro}$ and 0.02 $\frac{1}{ms}$ for $k_{f,Glu,post}$. Thus, also in the new synapse model, the same fraction of glutamate (80 %) is left into the synaptic cleft.

The amount of glutamate released into the synaptic cleft is generally assumed to exceed the need for receptor activation. Thus, the 80 % of the glutamate concentration that was left to activate the receptors was more than enough, and not all of it was used for activating the receptors in the model. However, given the limited time, keeping the share of total consumption of glutamate the same as in the original synapse model was the most rational way to optimize the glutamate dynamics in the synaptic cleft. This approach required minimal changes in the original and already validated values describing the glutamate dynamics in the synaptic cleft. With more time, the values could be changed if new experimental data will become available, and re-validation of the values can be performed.

The new variable Glu_{astro} (Figure 4.1) describes the intracellular glutamate concentration in the astrocyte. When comparing the variation in this concentration value to the pulse-like responses of neuronal model variables (for example in Figures 4.3L–N and 4.5L–N), the trend of the signaling seems to be slower. This follows the general understanding that the Ca^{2+} signaling-mediated astrocytic mechanisms are slower compared to, for example, neuronal glutamate release. In the new model, Glu_{astro} is dependent on the astrocytic glutamate uptake rates from the synaptic cleft and extrasynaptic space, but also on the amount of glutamate released from the astrocyte. As seen from Figure 4.1, the astrocytic

glutamate concentration increased with time and did not reach 0 μM after the simulation started. The only mechanism for glutamate consumption described in the astrocytic component of the new model was the release of glutamate. The remaining glutamate concentration in the astrocyte could therefore be considered to describe the glutamate that is used in other intracellular processes in the brain.

In the original synapse model, the released glutamate from astrocyte, and thus also the variable $[Glu]_{extsyn}$ (according to the Equation (3.5)), is dependent on a constant parameter G_{astro}. To reproduce similar glutamate release rate, the variation of $[Glu]_{astro}$ had to be fitted to reach similar scales than the value of G_{astro}. This was challenging, because the uptake rate $v_{Glu,uptake,astro}$ was also restricted by the glutamate concentration in the synaptic cleft and did not at first reach the required level. This was solved with a scaling factor ($r_{cleft,astro}$ in Equation (4.3)) describing the ratio between the volume of synaptic cleft and the volume of astrocyte. This value was fitted purely to produce the required uptake level, and it is not based on previous studies or experimental data on the ratio between those volumes. When continuing the development of glutamate dynamics in the synaptic cleft, also this scaling factor could be improved to realistically describe the ratio of the volumes of synaptic cleft and astrocyte.

As seen from the resulting equations, the scheme of describing the glutamate dynamics in the models by Tewari and Majumdar [90] and Blanchard et al. [93] was very compatible with the scheme of the original synapse model, allowing the implementation to be very consistent with their way of modeling it. This was beneficial for the success of the development process during a limited period of time. The new model was mainly evaluated by comparing the representations of the model dynamics qualitatively using visual inspection between the new and original models. In the time frame used for this work, this was the most efficient way to do so. The original model and its components were carefully evaluated against previous experimental data, and since the main aim of this work was to develop a functioning component for astrocytic glutamate uptake, this level of comparison was justifiable. In addition, most of the developed equations were based on previous studies that have been published. The new model can be validated when more experimental data for astrocytic glutamate uptake and related parameters become available.

Comparison of Figures 4.2, 4.3, 4.4 and 4.5 shows that the new model performed almost similarly compared to the original synapse model. However, in the new model, the intracellular astrocytic glutamate concentration was described as a differential equation, making its response dynamical. This also affected the concentration of the glutamate released from the astrocyte. In the original synapse model (Figure 4.4), the increases in the extrasynaptic concentrations were of constant magnitude. In the new synapse model (Figure 4.5), the release of glutamate to the extrasynaptic space increased with time, responding to the increasing trend of the astrocytic glutamate concentration (Figure 4.1).

However, even the smaller increases of extrasynaptic glutamate concentration, together with the spillover of glutamate from the synaptic cleft, were enough to activate the presynaptic Ca^{2+} and CaN concentrations almost identically compared to the responses of the original synapse model.

Furthermore, additional increases of glutamate concentration in the extrasynaptic space were observed with the temporal difference of ΔT=$-$150ms (Figure 4.5L). This led also to additional pulses in the activation of the presynaptic Ca^{2+} (Figure 4.5M) and CaN concentration (Figure 4.5N). When observing the developed component for glutamate uptake pathway and the modification required to implement it, the most likely explanation for this is that the astrocytic Ca^{2+} signaling reaches its threshold value more frequently. The signaling cascades affecting the astrocytic Ca^{2+} signaling, including the activation of the postsynaptic endocannabinoid production as well as the astrocytic glutamate concentration, was fitted to the corresponding original levels as closely as possible. Even small deviations in the endocannabinoid concentration, hardly seen from the graphical presentations, can lead to an additional Ca^{2+} signaling pulses to exceed the threshold value. In the new model, the astrocytic glutamate concentration $[Glu]_{astro}$ was described with a differential equation that depended on other parameters and variables, whereas in the original synapse model it was presented with a constant parameter G_{astro}. Due to the dynamically increasing nature of the variable $[Glu]_{astro}$, it was not possible to reach exactly the value of G_{astro}. Based on the analysis performed during this thesis work, this dynamical change did not significantly affect the work.

The new model performed well when considering the complexity of the original model, and the inevitable differences in dynamics due to replacing constant values with differential equations. The main aim of this work was to create the astrocytic glutamate uptake component and achieve appropriate level of function. The aim was reached, which also showed that additional components can be added to the original synapse model. From now on, the model development can be continued with more certainty.

The evaluation of the new synapse model continued with simulations of three different conditions: (1) astrocytic glutamate uptake rate was increased, (2) astrocytic glutamate uptake rate was decreased, and (3) astrocytic glutamate uptake was blocked. It was of interest to see whether the function of the new implementation was logical even when deviating from the optimized performance, where the dynamics was fitted to the original model. Further evaluation could also give some initial views of how this new component of astrocytic glutamate uptake could be used to study the neuron-astrocyte interactions at the synapse.

When the rate of astrocytic glutamate uptake was increased (Figure 4.7), the glutamate clearance from the synaptic cleft into the astrocyte was faster. This led to a situation where there was not enough glutamate to be used for activating the postsynaptic recep-

tors, further leading to a decrease in the activation of postsynaptic intracellular signaling cascades leading to the release of 2-AG. Finally, this caused decreased activation of astrocytic Ca^{2+} which affected the glutamate release. An increase in the astrocytic glutamate uptake rate and intracellular concentration, compared to the baseline of this model implementation, can be seen when comparing Figures 4.1 and 4.6.

The opposite condition was when the rate of astrocytic glutamate uptake was decreased (Figure 4.9). This led to slower clearance of glutamate uptake, during which the postsynaptic receptors were excessively activated. Excess activation of receptors led to an increase in the postsynaptic intracellular signaling cascades, increasing the amount of released 2-AG. This then increased the astrocytic Ca^{2+} oscillations. The astrocytic Ca^{2+} and IP_3 responses to the increases in the postsynaptic 2-AG seemed to perform unrealistically during the first pulse. The decrease in the astrocytic glutamate uptake rate and intracellular concentration, compared to the baseline of this model implementation, can be seen when comparing Figures 4.1 and 4.8.

When the astrocytic glutamate uptake was completely blocked (Figure 4.11), the model performance changed completely. There was a significant deviation with each temporal difference due to the lack of glutamate taken into the astrocyte. The glutamate uptake from the extrasynaptic space is small, as seen from Figure 4.10. This uptake from extrasynaptic space does not provide enough astrocytic glutamate to carry out the mechanism of astrocytic glutamate release. For this reason, the presynaptic neuron was not activated as much as in the previous conditions when the glutamate uptake from the synaptic cleft to the astrocyte existed. In addition, the first pulse-like responses of the variables presenting postsynaptic 2-AG, and astrocytic Ca^{2+} and IP_3 concentrations seemed to behave rather uncontrollably. Even so, the trend itself seemed plausible, since the excessive activation of postsynaptic signaling cascades caused significant increase in the astrocytic Ca^{2+} signaling. However, to study whether the effect is fully biologically realistic would require more evaluation.

Despite some of the first pulse-like responses seemed to behave uncontrollably, the overall performance of the new implementation in the three presented conditions (1–3) seemed to follow the expected trends. The model predicted such consequences for the increase, decrease and blocking of astrocytic glutamate uptake that could be also biologically realistic. However, without suitable experimental data, the accuracy of the magnitude and timing of the signaling cannot be addressed. This does, however, give important preliminary information about the possible range of tests that can be performed with this specific model. These three conditions could also represent possible impairments of astrocytic glutamate uptake in disease.

The model development process concentrated on creating the component for glutamate uptake pathway from the synaptic cleft to the astrocyte. After comprehensive validation of

the model, some details should be addressed in the future. It is of interest to evaluate, for example, how much the increased or decreased astrocytic glutamate uptake rates directly affect the astrocytic Ca^{2+} signaling. In the new model, the intracellular glutamate concentration of astrocyte did not affect its own Ca^{2+} concentrations, and thus the changes in the uptake rate only had an indirect effect through affecting the postsynaptic 2-AG production. Currently, it is not known how the model would perform if the intracellular astrocytic signaling cascades were connected in more detail.

Another suggestion is to continue the model development and study the role of glutamate dynamics in neuron-astrocyte interactions by implementing an uptake pathway also into the presynaptic neuron. In the current version of the model, the receptors in the presynaptic neuron are activated by the extrasynaptic glutamate concentration, but it does not affect the glutamate concentration inside the presynaptic neuron. By adding expression also for the presynaptic glutamate uptake, the recycling of glutamate could be completed, making the synapse model even more inclusive.

6. CONCLUSIONS

This thesis work presented a new developed component for astrocytic glutamate uptake from the synaptic cleft to the astrocyte. The component was integrated into the previously published neuron-astrocyte synapse model describing the phenomenon leading to spike-timing-dependent long-term depression. The original synapse model did not incorporate a direct astrocytic glutamate uptake pathway from the synaptic cleft, and the related astrocytic intracellular glutamate dynamics were controlled with a constant concentration parameter. The aim of this thesis work was to integrate the new glutamate uptake component into the original model, while reproducing the original model dynamics as closely as possible. This goal was reached, and it enabled also further testing of the new synapse model. The model behavior could be examined with computationally simulating different impaired conditions, where the rate of the astrocytic glutamate uptake was modified by increasing, decreasing and blocking it. The new developed model performed as expected in these different conditions, supporting the robustness of the new implementation. In the future, other, similar conditions could be stimulated to employ the new synapse model to study the role of astrocytic glutamate uptake in health and disease.

In addition to the original synapse model, the materials and methods for this thesis work included a comprehensive survey of currently available glutamate transporter models. This survey resulted in over 40 models incorporating glutamate uptake component, however revealing a significant gap in the replicability of these models. The simulation codes were available for only one sixth of the models. Even though most of the model equations were presented, the important implementation details were missing. In addition to presenting the modified and developed equations for the new synapse model, also the implementation details required to replicate the model were presented in this thesis work. Currently, there are not such established mathematical expressions for describing astrocyte dynamics, like glutamate uptake, compared to neuronal modeling. To create an optimal base to advance the modeling of astrocytes, more completely accessible and available models are required.

Even though this thesis work presented a successful component for astrocytic glutamate uptake for a neuron-astrocyte synapse model, a completely validated model most likely requires years of work and research. However, the presented results showed that such a component for astrocytic glutamate uptake could be integrated afterwards without need-

ing to recreate the whole synapse model, leaving optimistic view for the model development process to advance the original synapse model. The next step forward could be, for example, implementing a direct pathway for presynaptic glutamate transport, and thus completing the modeling of the glutamate-glutamine cycle.

REFERENCES

[1] T. Trappenberg, *Fundamentals of Computational Neuroscience*. OUP Oxford, 2009.

[2] E. Zisis *et al.*, “Digital reconstruction of the neuro-glia-vascular architecture”, *Cerebral Cortex*, vol. 31, no. 12, pp. 5686–5703, 2021.

[3] M. Nedergaard, B. Ransom, and S. A. Goldman, “New roles for astrocytes: Redefining the functional architecture of the brain”, *Trends in Neurosciences*, vol. 26, no. 10, pp. 523–530, 2003.

[4] D. P. Pelvig, H. Pakkenberg, A. K. Stark, and B. Pakkenberg, “Neocortical glial cell numbers in human brains”, *Neurobiology of Aging*, vol. 29, no. 11, pp. 1754–1762, 2008.

[5] S. Herculano-Houzel, “The glia/neuron ratio: How it varies uniformly across brain structures and species and what that means for brain physiology and evolution”, *Glia*, vol. 62, no. 9, pp. 1377–1391, 2014.

[6] D. Wang and A. Bordey, “The astrocyte odyssey”, *Progress in Neurobiology*, vol. 86, no. 4, pp. 342–367, 2008.

[7] R. Min and T. Nevian, “Astrocyte signaling controls spike timing–dependent depression at neocortical synapses”, *Nature Neuroscience*, vol. 15, no. 5, pp. 746–753, 2012.

[8] M. Navarrete *et al.*, “Astrocytes mediate in vivo cholinergic-induced synaptic plasticity”, *PLoS Biology*, vol. 10, no. 2, e1001259, 2012.

[9] R. A. Hawkins, “The blood-brain barrier and glutamate”, *The American Journal of Clinical Nutrition*, vol. 90, no. 3, 867S–874S, 2009.

[10] K. Tanaka *et al.*, “Epilepsy and exacerbation of brain injury in mice lacking the glutamate transporter glt-1”, *Science*, vol. 276, no. 5319, pp. 1699–1702, 1997.

[11] T. Manninen, A. Saudargiene, and M.-L. Linne, “Astrocyte-mediated spike-timing-dependent long-term depression modulates synaptic properties in the developing cortex”, *PLoS Computational Biology*, vol. 16, no. 11, e1008360, 2020.

[12] L. Squire, D. Berg, F. E. Bloom, S. Du Lac, A. Ghosh, and N. C. Spitzer, *Fundamental Neuroscience*. Academic Press, 2012.

[13] Q. Zhang, Y. Zeng, T. Zhang, and T. Yang, “Comparison between human and rodent neurons for persistent activity performance: A biologically plausible computational investigation”, *Frontiers in Systems Neuroscience*, p. 98, 2021.

[14] G. A. Ascoli, “Mobilizing the base of neuroscience data: The case of neuronal morphologies”, *Nature Reviews Neuroscience*, vol. 7, no. 4, pp. 318–324, 2006.

[15] R. Benavides-Piccione *et al.*, “Differential structure of hippocampal ca1 pyramidal neurons in the human and mouse”, *Cerebral Cortex*, vol. 30, no. 2, pp. 730–752, 2020.

[16] C. A. Kadgien, A. Kamesh, and A. J. Milnerwood, “Endosomal traffic and glutamate synapse activity are increased in vps35 d620n mutant knock-in mouse neurons, and resistant to lrrk2 kinase inhibition”, *Molecular brain*, vol. 14, no. 1, pp. 1–20, 2021.

[17] C. Koch, *Biophysics of Computation: Information processing in single neurons*. Oxford university press, 1999.

[18] Y. Zhou and N. C. Danbolt, “Glutamate as a neurotransmitter in the healthy brain”, *Journal of Neural Transmission*, vol. 121, no. 8, pp. 799–817, 2014.

[19] G. M. Shepherd, *Neurobiology*. Oxford University Press, 1988.

[20] S. E. Brotherson, *Understanding brain development in young children*. Citeseer, 2005.

[21] D. Sterratt, B. Graham, A. Gillies, and D. Willshaw, *Principles of computational modelling in neuroscience*. Cambridge University Press, 2011.

[22] V. Eulenburg and J. Gomeza, “Neurotransmitter transporters expressed in glial cells as regulators of synapse function”, *Brain Research Reviews*, vol. 63, no. 1-2, pp. 103–112, 2010.

[23] N. T. Carnevale and M. L. Hines, *The NEURON book*. Cambridge University Press, 2006.

[24] M.-O. Gewaltig and M. Diesmann, “Nest (neural simulation tool)”, *Scholarpedia*, vol. 2, no. 4, p. 1430, 2007.

[25] A. L. Hodgkin and A. F. Huxley, “A quantitative description of membrane current and its application to conduction and excitation in nerve”, *The Journal of Physiology*, vol. 117, no. 4, p. 500, 1952.

[26] R. A. McDougal *et al.*, “Twenty years of modeldb and beyond: Building essential modeling tools for the future of neuroscience”, *Journal of Computational Neuroscience*, vol. 42, no. 1, pp. 1–10, 2017.

[27] A. Volterra and J. Meldolesi, “Astrocytes, from brain glue to communication elements: The revolution continues”, *Nature Reviews Neuroscience*, vol. 6, no. 8, pp. 626–640, 2005.

[28] A. Verkhratsky and M. Nedergaard, “Physiology of astroglia”, *Physiological Reviews*, vol. 98, no. 1, pp. 239–389, 2018.

[29] R. Cabezas *et al.*, “Astrocytic modulation of blood brain barrier: Perspectives on parkinson’s disease”, *Frontiers in Cellular Neuroscience*, vol. 8, p. 211, 2014.

[30] E. Lee and W.-S. Chung, “Glial control of synapse number in healthy and diseased brain”, *Frontiers in Cellular Neuroscience*, vol. 13, p. 42, 2019.

[31] M. M. Halassa and P. G. Haydon, “Integrated brain circuits: Astrocytic networks modulate neuronal activity and behavior”, *Annual Review of Physiology*, vol. 72, pp. 335–355, 2010.

[32] R. D. Fields and B. Stevens-Graham, “New insights into neuron-glia communication”, *Science*, vol. 298, no. 5593, pp. 556–562, 2002.

[33] M.-L. Linne, J. Aćimović, A. Saudargiene, and T. Manninen, “Neuron–glia interactions and brain circuits”, in *Computational Modelling of the Brain*, Springer, 2022, pp. 87–103.

[34] D. Attwell, A. M. Buchan, S. Charpak, M. Lauritzen, B. A. MacVicar, and E. A. Newman, “Glial and neuronal control of brain blood flow”, *Nature*, vol. 468, no. 7321, pp. 232–243, 2010.

[35] N. A. Oberheim *et al.*, “Uniquely hominid features of adult human astrocytes”, *Journal of Neuroscience*, vol. 29, no. 10, pp. 3276–3287, 2009.

[36] W. Xin *et al.*, “Ventral midbrain astrocytes display unique physiological features and sensitivity to dopamine d2 receptor signaling”, *Neuropsychopharmacology*, vol. 44, no. 2, pp. 344–355, 2019.

[37] G. M. McKhann, R. D’Ambrosio, and D. Janigro, “Heterogeneity of astrocyte resting membrane potentials and intercellular coupling revealed by whole-cell and gramicidin-perforated patch recordings from cultured neocortical and hippocampal slice astrocytes”, *Journal of Neuroscience*, vol. 17, no. 18, pp. 6850–6863, 1997.

[38] M. Zhou and H. K. Kimelberg, “Freshly isolated astrocytes from rat hippocampus show two distinct current patterns and different [k+] uptake capabilities”, *Journal of Neurophysiology*, vol. 84, no. 6, pp. 2746–2757, 2000.

[39] K. Ryoo and J. Park, “Two-pore domain potassium channels in astrocytes”, *Experimental Neurobiology*, vol. 25, no. 5, p. 222, 2016.

[40] L. W. Pappalardo, J. A. Black, and S. G. Waxman, “Sodium channels in astroglia and microglia”, *Glia*, vol. 64, no. 10, pp. 1628–1645, 2016.

[41] J. McNeill, C. Rudyk, M. Hildebrand, and N. Salmaso, “Ion channels and electrophysiological properties of astrocytes: Implications for emergent stimulation technologies”, *Frontiers in Cellular Neuroscience*, vol. 15, p. 183, 2021.

[42] N. Bazargani and D. Attwell, “Astrocyte calcium signaling: The third wave”, *Nature Neuroscience*, vol. 19, no. 2, pp. 182–189, 2016.

[43] A. H. Cornell-Bell, S. M. Finkbeiner, M. S. Cooper, and S. J. Smith, “Glutamate induces calcium waves in cultured astrocytes: Long-range glial signaling”, *Science*, vol. 247, no. 4941, pp. 470–473, 1990.

[44] V. Parpura, T. A. Basarsky, F. Liu, K. Jeftinija, S. Jeftinija, and P. G. Haydon, “Glutamate-mediated astrocyte–neuron signalling”, *Nature*, vol. 369, no. 6483, pp. 744–747, 1994.

[45] J. W. Dani, A. Chernjavsky, and S. J. Smith, “Neuronal activity triggers calcium waves in hippocampal astrocyte networks”, *Neuron*, vol. 8, no. 3, pp. 429–440, 1992.

[46] S. Kriegler and S. Chiu, “Calcium signaling of glial cells along mammalian axons”, *Journal of Neuroscience*, vol. 13, no. 10, pp. 4229–4245, 1993.

[47] A. Araque, V. Parpura, R. P. Sanzgiri, and P. G. Haydon, “Glutamate-dependent astrocyte modulation of synaptic transmission between cultured hippocampal neurons”, *European Journal of Neuroscience*, vol. 10, no. 6, pp. 2129–2142, 1998.

[48] A. Araque, V. Parpura, R. P. Sanzgiri, and P. G. Haydon, “Tripartite synapses: Glia, the unacknowledged partner”, *Trends in Neurosciences*, vol. 22, no. 5, pp. 208–215, 1999.

[49] N. B. Hamilton and D. Attwell, “Do astrocytes really exocytose neurotransmitters?”, *Nature Reviews Neuroscience*, vol. 11, no. 4, pp. 227–238, 2010.

[50] S. Guerra-Gomes, N. Sousa, L. Pinto, and J. F. Oliveira, “Functional roles of astrocyte calcium elevations: From synapses to behavior”, *Frontiers in Cellular Neuroscience*, vol. 11, p. 427, 2018.

[51] M. De Pittà and N. Brunel, “Modulation of synaptic plasticity by glutamatergic gliotransmission: A modeling study.”, *Neural Plasticity*, 2016.

[52] G. L. Collingridge, S. Peineau, J. G. Howland, and Y. T. Wang, “Long-term depression in the cns”, *Nature Reviews Neuroscience*, vol. 11, no. 7, pp. 459–473, 2010.

[53] T. Manninen, R. Havela, and M.-L. Linne, “Computational models for calcium-mediated astrocyte functions”, *Frontiers in Computational Neuroscience*, vol. 12, p. 14, 2018.

[54] X. Yu, J. Nagai, and B. S. Khakh, “Improved tools to study astrocytes”, *Nature Reviews Neuroscience*, vol. 21, no. 3, pp. 121–138, 2020.

[55] L. P. Savtchenko *et al.*, “Disentangling astroglial physiology with a realistic cell model in silico”, *Nature Communications*, vol. 9, no. 1, pp. 1–15, 2018.

[56] Y.-X. Li and J. Rinzel, “Equations for insp3 receptor-mediated [ca^{2+}] i oscillations derived from a detailed kinetic model: A hodgkin-huxley like formalism”, *Journal of Theoretical Biology*, vol. 166, no. 4, pp. 461–473, 1994.

[57] M. V. Bennett and R. S. Zukin, “Electrical coupling and neuronal synchronization in the mammalian brain”, *Neuron*, vol. 41, no. 4, pp. 495–511, 2004.

[58] U. Pannasch, M. Derangeon, O. Chever, and N. Rouach, “Astroglial gap junctions shape neuronal network activity”, *Communicative and Integrative Biology*, vol. 5, no. 3, pp. 248–254, 2012.

[59] N. C. Danbolt, “Glutamate uptake”, *Progress in Neurobiology*, vol. 65, no. 1, pp. 1–105, 2001.

[60] H. Markram, W. Gerstner, and P. J. Sjöström, “A history of spike-timing-dependent plasticity”, *Frontiers in Synaptic Neuroscience*, vol. 3, p. 4, 2011.

[61] N. Deperrois and M. Graupner, “Short-term depression and long-term plasticity together tune sensitive range of synaptic plasticity”, *PLoS Computational Biology*, vol. 16, no. 9, e1008265, 2020.

[62] H. Markram, W. Gerstner, and P. J. Sjöström, “Spike-timing-dependent plasticity: A comprehensive overview”, *Frontiers in Synaptic Neuroscience*, vol. 4, p. 2, 2012.

[63] H. Markram, J. Lübke, M. Frotscher, and B. Sakmann, “Regulation of synaptic efficacy by coincidence of postsynaptic aps and epsps”, *Science*, vol. 275, no. 5297, pp. 213–215, 1997.

[64] G.-q. Bi and M.-m. Poo, “Synaptic modifications in cultured hippocampal neurons: Dependence on spike timing, synaptic strength, and postsynaptic cell type”, *Journal of Neuroscience*, vol. 18, no. 24, pp. 10 464–10 472, 1998.

[65] E. E. Benarroch, “Neuron-astrocyte interactions: Partnership for normal function and disease in the central nervous system”, in *Mayo Clinic Proceedings*, Elsevier, vol. 80, 2005, pp. 1326–1338.

[66] E. A. Newman, “New roles for astrocytes: Regulation of synaptic transmission”, *Trends in Neurosciences*, vol. 26, no. 10, pp. 536–542, 2003.

[67] A. Zador, C. Koch, and T. H. Brown, “Biophysical model of a hebbian synapse.”, *Proceedings of the National Academy of Sciences*, vol. 87, no. 17, pp. 6718–6722, 1990.

[68] T. Manninen, K. Hituri, J. H. Kotaleski, K. T. Blackwell, and M.-L. Linne, “Postsynaptic signal transduction models for long-term potentiation and depression”, *Frontiers in Computational Neuroscience*, vol. 4, p. 152, 2010.

[69] M. V. Tsodyks and H. Markram, “The neural code between neocortical pyramidal neurons depends on neurotransmitter release probability”, *Proceedings of the National Academy of Sciences*, vol. 94, no. 2, pp. 719–723, 1997.

[70] M. Tsodyks, K. Pawelzik, and H. Markram, “Neural networks with dynamic synapses”, *Neural Computation*, vol. 10, no. 4, pp. 821–835, 1998.

[71] J. Clements, “Transmitter timecourse in the synaptic cleft: Its role in central synaptic function”, *Trends in Neurosciences*, vol. 19, no. 5, pp. 163–171, 1996.

[72] D. N. Chiu and C. E. Jahr, “Extracellular glutamate in the nucleus accumbens is nanomolar in both synaptic and non-synaptic compartments”, *Cell Reports*, vol. 18, no. 11, pp. 2576–2583, 2017.

[73] D. A. Coulter and T. Eid, “Astrocytic regulation of glutamate homeostasis in epilepsy”, *Glia*, vol. 60, no. 8, pp. 1215–1226, 2012.

[74] X.-x. Dong, Y. Wang, and Z.-h. Qin, “Molecular mechanisms of excitotoxicity and their relevance to pathogenesis of neurodegenerative diseases”, *Acta Pharmacologica Sinica*, vol. 30, no. 4, pp. 379–387, 2009.

[75] S. Mahmoud, M. Gharagozloo, C. Simard, and D. Gris, “Astrocytes maintain glutamate homeostasis in the cns by controlling the balance between glutamate uptake and release”, *Cells*, vol. 8, no. 2, p. 184, 2019.

[76] M. Ankarcrona *et al.*, “Glutamate-induced neuronal death: A succession of necrosis or apoptosis depending on mitochondrial function”, *Neuron*, vol. 15, no. 4, pp. 961–973, 1995.

[77] C. M. Anderson and R. A. Swanson, “Astrocyte glutamate transport: Review of properties, regulation, and physiological functions”, *Glia*, vol. 32, no. 1, pp. 1–14, 2000.

[78] C. R. Rose, D. Ziemens, V. Untiet, and C. Fahlke, “Molecular and cellular physiology of sodium-dependent glutamate transporters”, *Brain Research Bulletin*, vol. 136, pp. 3–16, 2018.

[79] C. Grewer and T. Rauen, “Electrogenic glutamate transporters in the cns: Molecular mechanism, pre-steady-state kinetics, and their impact on synaptic signaling”, *The Journal of Membrane Biology*, vol. 203, no. 1, pp. 1–20, 2005.

[80] S. Holmseth *et al.*, “The density of eaac1 (eaat3) glutamate transporters expressed by neurons in the mammalian cns”, *Journal of Neuroscience*, vol. 32, no. 17, pp. 6000–6013, 2012.

[81] Y. Dehnes, F. A. Chaudhry, K. Ullensvang, K. P. Lehre, J. Storm-Mathisen, and N. C. Danbolt, “The glutamate transporter eaat4 in rat cerebellar purkinje cells: A glutamate-gated chloride channel concentrated near the synapse in parts of the dendritic membrane facing astroglia”, *Journal of Neuroscience*, vol. 18, no. 10, pp. 3606–3619, 1998.

[82] D. V. Pow and N. L. Barnett, “Developmental expression of excitatory amino acid transporter 5: A photoreceptor and bipolar cell glutamate transporter in rat retina”, *Neuroscience Letters*, vol. 280, no. 1, pp. 21–24, 2000.

[83] K. P. Lehre, L. M. Levy, O. P. Ottersen, J. Storm-Mathisen, and N. C. Danbolt, “Differential expression of two glial glutamate transporters in the rat brain: Quantitative and immunocytochemical observations”, *Journal of Neuroscience*, vol. 15, no. 3, pp. 1835–1853, 1995.

[84] N. Zerangue and M. P. Kavanaugh, “Flux coupling in a neuronal glutamate transporter”, *Nature*, vol. 383, no. 6601, pp. 634–637, 1996.

[85] M. Erecińska and I. A. Silver, “Metabolism and role of glutamate in mammalian brain”, *Progress in Neurobiology*, vol. 35, no. 4, pp. 245–296, 1990.

[86] J. L. Stobart and C. M. Anderson, “Multifunctional role of astrocytes as gatekeepers of neuronal energy supply”, *Frontiers in Cellular Neuroscience*, vol. 7, p. 38, 2013.

[87] S. J. Mitchell and R. A. Silver, “Glutamate spillover suppresses inhibition by activating presynaptic mglurs”, *Nature*, vol. 404, no. 6777, pp. 498–502, 2000.

[88] J. Shen, “Modeling the glutamate–glutamine neurotransmitter cycle”, *Frontiers in Neuroenergetics*, vol. 5, p. 1, 2013.

[89] A. N. Silchenko and P. A. Tass, “Computational modeling of paroxysmal depolarization shifts in neurons induced by the glutamate release from astrocytes”, *Biological Cybernetics*, vol. 98, no. 1, pp. 61–74, 2008.

[90] S. Tewari and K. Majumdar, “A mathematical model for astrocytes mediated ltp at single hippocampal synapses”, *Journal of Computational Neuroscience*, vol. 33, no. 2, pp. 341–370, 2012.

[91] G. Perea and A. Araque, “Astrocytes potentiate transmitter release at single hippocampal synapses”, *Science*, vol. 317, no. 5841, pp. 1083–1086, 2007.

[92] S. L. Allam *et al.*, “A computational model to investigate astrocytic glutamate uptake influence on synaptic transmission and neuronal spiking”, *Frontiers in Computational Neuroscience*, vol. 6, p. 70, 2012.

[93] S. Blanchard *et al.*, “A new computational model for neuro-glio-vascular coupling: Astrocyte activation can explain cerebral blood flow nonlinear response to interictal events”, *PLoS ONE*, vol. 11, no. 2, e0147292, 2016.

[94] J. Li, J. Tang, J. Ma, M. Du, R. Wang, and Y. Wu, “Dynamic transition of neuronal firing induced by abnormal astrocytic glutamate oscillation”, *Scientific Reports*, vol. 6, no. 1, pp. 1–10, 2016.

[95] C. Conte, R. Lee, M. Sarkar, and D. Terman, “A mathematical model of recurrent spreading depolarizations”, *Journal of Computational Neuroscience*, vol. 44, no. 2, pp. 203–217, 2018.

[96] B. Flanagan, L. McDaid, J. Wade, K. Wong-Lin, and J. Harkin, “A computational study of astrocytic glutamate influence on post-synaptic neuronal excitability”, *PLoS Computational Biology*, vol. 14, no. 4, e1006040, 2018.

[97] M. Kalia, H. G. Meijer, S. A. van Gils, M. J. van Putten, and C. R. Rose, “Ion dynamics at the energy-deprived tripartite synapse”, *PLoS Computational Biology*, vol. 17, no. 6, e1009019, 2021.

[98] B. Kim, S. L. Hawes, F. Gillani, L. J. Wallace, and K. T. Blackwell, “Signaling pathways involved in striatal synaptic plasticity are sensitive to temporal pattern and exhibit spatial specificity”, *PLoS Computational Biology*, vol. 9, no. 3, e1002953, 2013.

[99] A. Perrillat-Mercerot, N. Bourmeyster, C. Guillevin, A. Miranville, and R. Guillevin, “Analysis of a mathematical model for the glutamate/glutamine cycle in the brain”, *Bulletin of Mathematical Biology*, vol. 81, no. 10, pp. 4251–4270, 2019.